# Use of sensitivity analysis to diagnose forecasting system performance

Florence Rabier[1,2], Ernst Klinker[1], Gwenaelle Hello[2]
[1]ECMWF, [2]Météo-France

Summary : Sensitivity analysis can be performed using the adjoint model. An adjoint integration provides the sensitivity of one output parameter of a numerical model (one forecast aspect) to all input parameters (initial conditions, model parameters). In particular, the adjoint method has been used to calculate the sensitivity of short-range forecast errors to the initial conditions. The gradient of the energy of the day 2 forecast error with respect to the initial conditions can be interpreted as a sum of rapidly growing components of the analysis error. An analysis modified by subtracting an appropriately scaled vector, proportional to the gradient, provides initial conditions for a « sensitivity integration » that is used to diagnose the effect of initial-data errors on forecast errors. The sensitivity patterns are small-scale, middle or lower-tropospheric structures which are tilted in the vertical. The general pattern of these structures is known to be associated with the fastest possible growth of forecast error. When used as initial perturbations, they evolve rapidly into synoptic-scale structures, propagating both downstream and to higher atmospheric levels. On average, the sensitivity integration corrects for about a tenth of the day 2 forecast error, which indicates that indeed not all of the error is in the fastest-amplifying modes. But the fraction of the error corrected at day 2 is important for an improvement in the medium-range, as this fraction continues to grow substantially in the non-linear regime. The adjoint model can also be used in optimization problems related to the diagnosis of forecasting system performance. An iteration procedure minimizing the short-range forecast error leads, after some iterations, to so-called key analysis errors. These are estimates of the part of analysis errors that is largely responsible for the short-range forecast errors. The first step of the minimization procedure provides a scaled gradient of the two-day forecast errors. Performing a few more steps in the minimization provides better estimates of the analysis error in the directions spanned by the leading singular vectors of the tangent-linear model. On a case study it is shown that three steps provide key analysis increments which, when added to the analysis, both significantly improve the fit to the available data, and substantially improve the subsequent model integration. It does not appear to be beneficial to do more steps of the minimization because of the uncertainty in the definition of the short-range forecast error, and of approximations in the tangent-linear model. Key analysis errors represent an improved estimate of analysis errors compared to the scaled gradient of day-2 forecast errors. In particular the geographical distribution shows the stability dependence of the scaled gradient. The projection of the gradient on the fastest growing errors limits maximum sensitivity to the major baroclinic zones. The close correspondence of evolved key analysis errors and forecast errors shows that key analysis errors are more realistically projecting on to full analysis errors. Another application of the method is the real-time diagnostic of forecast behaviour based on a predefined forecast aspect such as the mean surface pressure in an area. The method consists in imposing at initial time a « sensitive » structure to the perturbation which is first computed by adjoint tools. The tuning of the perturbation amplitude is obtained by reducing the distance to the observations at the locations where the sensitive structure is of significant amplitude.

## 1. INTRODUCTION

The adjoint technique (LeDimet and Talagrand 1986) provides us with a tool to directly investigate the sensitivity of a forecast aspect to input parameters. The sensitivity to model parameters has been investigated, for instance, by Hall et al. (1982), Hall (1986), Marais and Musson-Genon (1992). The sensitivity of a forecast aspect to the initial conditions, has been the subject of various studies (Errico and Vukicevic 1992 ; Rabier et al. 1992 ; Errico et al. 1993 ; Langland et al. 1995 ; Oortwijn and Barkmeijer 1995 ; Horanyi and Joly 1996).

The adjoint model can also be used in optimization problems related to the diagnostic of forecasting system performance. Minimizing a forecast criterion (distance to observations for instance), one can get estimates of initial conditions, model parameters or model errors.

In section 2, the mathematical basis of the method is explained. Section 3 summarizes the results obtained by Rabier et al (1996) on the sensitivity of forecast errors to initial conditions. In section 4, the key analysis errors obtained by minimization of forecast errors as in Klinker et al (1998) are described. A real-time application of the method is presented in section 5, based on Hello et al (1999). Finally, section 6 concludes and gives other examples of applications of the adjoint technique to forecasting system performance issues.

## 2. THE ADJOINT MODEL : A TOOL FOR SENSITIVITY ANALYSIS

### 2.1 General formalism

Conventional sensitivity analysis consists in changing one aspect of input parameters (model parameters or initial conditions) and re-running the model. It gives the sensitivity of all output parameters to one change in the input parameters.

In contrast, adjoint sensitivity analysis consists in performing one adjoint integration starting from a defined output parameter (forecast aspect). It gives the sensitivity of one output parameter to all input parameters.

The mathematical basis for the adjoint method is explained below.

Let J(x) be a function of model variables x at time t.

One assumes the existence of $x=M(u)$, where $M$ is an operator linking u and x, and u is a vector of model parameters.

$\delta x=\mathbf{M}\delta u$: a perturbation $\delta u$ leads to $\delta x$, using 1st order Taylor expansion, where $\mathbf{M}$ is the tangent-linear operator of $M$ linearized in the vicinity of u.

$<.,.>_u$ and $<.,.>_x$ are inner-products in the spaces of parameters and model variables.

By definition of the gradient (vector of first-order derivatives of J with respect to x : $\nabla_x J$ )

$\delta J=J(x+\delta x)-J(x)=<\nabla_x J,\delta x>_x$ to first-order

$\delta J=<\nabla_x J,\mathbf{M}\delta u>_x$

And, by definition of the adjoint operator

$\delta J=<\mathbf{M}^*\nabla_x J,\delta u>_u$

which implies that $\nabla_u J= \mathbf{M}^*\nabla_x J$

The sensitivity of J with respect to u is obtained by applying the adjoint of the tangent-linear operator to the gradient of J with respect to x.

The limitation of the adjoint equations is that they are linear and can only describe the sensitivity to small initial perturbations for which the time evolution can be described by the tangent-linear model.

## 2.2 A simple example

The mathematics can be illustrated further by a simple example, given below

J is a function of model variables X=(x,y), $J=x^2+y^2$

The parameters are the initial conditions $X_0=(x_0,y_0)$

The model *M* is given by : $x = a\,x_0^2+b\,y_0^2$

$y = y_0$

The tangent-linear model **M**, linearization of *M* with respect to Xo is

T-L model **M**: $\delta x = 2ax_0 \,.\, \delta x_0 + 2by_0 \,.\, \delta y_0$

$\delta y = 0 \,.\, \delta x_0 + 1 \,.\, \delta y_0$

Considering the simple dot-products, the adjoint model **M*** is simply the transpose of **M**

Adjoint model **M***: $\delta x_0 *= 2ax_0 \,.\, \delta x^* + 0 \,.\, \delta y^*$

$\delta y_0 *= 2by_0 \,.\, \delta x^* + 1 \,.\, \delta y^*$

One can easily check that $\nabla_{x_0} J = \mathbf{M}^* \nabla_X J$:

$\nabla_X J = (2x, 2y)$

$\nabla_{X0} J = (\partial x/\partial x_0 \partial J/\partial x + \partial y/\partial x_0 \partial J/\partial y,\ \partial x/\partial y_0 \partial J/\partial x + \partial y/\partial y_0 \partial J/\partial y)$

$\nabla_{X0} J = (2ax_0 \partial J/\partial x + 0.\partial J/\partial y,\ 2by_0\, \partial J/\partial x + 1.\partial J/\partial y)$ which is exactly

$\nabla_{X0} J = \mathbf{M}^* \nabla_X J$

## 2.3 Sensitivity to model parameters

The sensitivity to various parameters can also be obtained.
Let us write

$x_n = M(x_{n-1},\alpha)$. Xn depends both on model variables Xn-1 at the previous time step of the model and on other model parameters $\alpha$.

$\delta x_n = \mathbf{M_{xn-1}} \delta x_{n-1} + \mathbf{M}_\alpha \delta\alpha$

$\delta x_n = \mathbf{M_{xn-1}M_{xn-2}...M_{x0}} \delta x_0 + (\mathbf{M_{xn-1}...M_{x0}} + ... + \mathbf{M_{xn-1}M_{xn-2}} + \mathbf{M_{xn-1}} + \mathbf{I})\mathbf{M}_\alpha \delta\alpha$

$\delta x_n$ is linked to $\delta\alpha$ by $\mathbf{M}_\alpha$ and $(\mathbf{M_{xi}})_i$ , contre $\mathbf{M}_\alpha$ is the first order derivative of **M** with respect to $\alpha$.

To compute the sensitivity with respect to $\alpha$, one needs the adjoints $\mathbf{M}^*_\alpha$ and $(\mathbf{M}^*_{\mathbf{xi}})_\mathbf{i}$

Errico and Vukicevic (1992), Rabier et al (1992), Langland et al (1995), Arbogast (1998),... investigated the sensitivity to initial conditions.

Another reference is Errico et al (1993) where they studied the sensitivity to initial conditions and lateral boundary conditions.

In the following sections, we will concentrate on the sensitivity of forecast errors to initial conditions.

# 3. SENSITIVITY OF FORECAST ERRORS TO INITIAL CONDITIONS

## 3.1 Expression and interpretation of gradient fields

In Rabier et al (1996) the diagnostic function is expressed as

$J(x)=1/2 \langle x-x^{ref}, x-x^{ref}\rangle$. It is a function of x at time t. $\langle .,. \rangle$ is the « energy » inner-product.

$\delta J=\langle x-x^{ref},\delta x\rangle=\langle x-x^{ref},\mathbf{M}\delta x_0\rangle=\langle \mathbf{M}^*(x-x^{ref}),\delta x_0\rangle$

which implies that $\nabla_{x0}J= \mathbf{M}^*\nabla_x J=\mathbf{M}^*(x-x^{ref})$

If one assumes that $x-x^{ref}$ represents the forecast error and that this forecast error is coming from the propagation of initial errors, $x-x^{ref}=\mathbf{M}e_0$, where $e_0$ is the initial analysis error, then

$\nabla_{x0}J=\mathbf{M}^* \mathbf{M}e_0$

Let us write $(v_i)$ the eigenvectors of $\mathbf{M}^* \mathbf{M}$ (singular vectors, which are used in the Ensemble Prediction System (Buizza et al., 1997)). If one expands $e_0$ on this basis :

$e_0=\sum e_i v_i$ , and

$\nabla_{x0}J=\sum \lambda_i^2 e_i v_i$

The gradient is dominated by the most unstable components of the analysis error (large $\lambda_i$'s)because these are directions along which the forecast error is likely to vary the most.

By definition of the gradient, perturbations of the form $\delta x_0=\alpha\nabla_{x0}J$ optimize the first-order change in J for a given norm of the perturbation $||\,\delta x_0\,||$.

One can also compute an optimal step-size for a quadratic J such as the one defining the forecast error in this example.

One can compute $\alpha$ such that $x_1= x_0-\alpha\nabla_{x0}J$ leads to the largest change in J

The Taylor expansion for $J(x_1)$ is

$J(x_1) = J(x_0) +\nabla_{x0}J^T (x_1-x_0) +1/2 (x_1-x_0)^T H (x_1-x_0)$

where H is the Hessian (matrix of second derivatives of J).

Setting $\partial J/\partial\alpha\ (x_1) = 0$ leads to

$\alpha = (\nabla_{x0}J^T\nabla_{x0}J)(\nabla_{x0}J^T H\nabla_{x0}J)^{-1}$

H can be computed from $\nabla_{x0}J$ and $\nabla_{xt}J$ : $\nabla_{xt}J-\nabla_{x0}J = H\ (x_t-x_0)$ where $x_t$ is a trial point. On can then see that from the computation of $J(x_0)$, $\nabla J(x_0)$, and of $J(x_t)$, $\nabla J(x_t)$ at a trial point, the optimal factor $\alpha$ can be computed leading the maximum decrease in J.

### 3.2 Experimental procedure

The diagnostic function J considered is the two-day forecast error computed over the latitude band [30N, 90N] :

$J(x^a) = 1/2\,||\ M(x^a) - x^{ref}\ ||^2$ where

$M$ is the nonlinear model (resolution T213L31), $x^a$ is the initial analysis, $x^{ref}$ is the verifying analysis, two days later.

The gradient with respect to $x^a$ is

$\nabla_{xa}J = \mathbf{M}^*(M(x^a) - x^{ref})$

$\mathbf{M}^*$ is the adjoint model computed at resolution T63L31 with simplified physics (vertical diffusion), along a trajectory at T63L31 with full physics.

The forecast experimentation consists of a control forecast from $x^a$ run at T106L31, and a sensitivity integration from $x^a - \alpha\nabla_{xa}J$ at T106L31, with $\alpha = 1/100$. This factor was close to optimal, although deduced from trial and error.

### 3.3 Results

Many cases of poor forecast performance (particularly over Europe) have been investigated by using the sensitivity calculations to modify the initial conditions. The consistent improvement of forecast skill in all cases proves the usefulness of this approach as a diagnostic tool to identify possible regions of analysis problems leading to major forecast failures. An interesting case occured on 6 April 1994 when the two-day forecast error was particularly sensitive to initial conditions in a region of relatively high data density over North America. Figure 1 shows the operational initialized analysis at 400 hPa (dotted lines) and the perturbed analysis (solid lines) ; the available radiosonde data are also shown. The perturbations derived from the sensitivity calculations produce a sharper upper air trough to the south-west of the Great Lakes which seems to be supported by data. The largest modifications to the analysis occur near (40°N, 96°W). The modifications improve the fit of the initial conditions to the available observations at 400 hPa in that area. For instance, the standard deviation of the difference between the analyses and the radiosonde measurements of the geopotential (« height ») of the 400 hPa surface in the region (50°N : 30°N, 110°W : 80°W) displayed in Fig. 1 is reduced from 20 to 19.5 gpm.

The time evolution of the streamfunction of the sensitivity perturbations (shown in Fig. 2 as a sequence of west-east cross sections at 12-hour intervals), exhibits the typical features of a very unstable baroclinic wave (Farrell 1990). The initial strong tilt in the vertical is also typical of the fastest growing perturbations of the ensemble prediction system (Buizza and Palmer, 1994). During the first 36 hours (Figs. 2 (a)-(d)) the growth is very much restricted to low levels, and the westward tilt with height decreases gradually with time. However, as the perturbation extends to larger horizontal and vertical scales (Figs. 2 (e) and (f)), the vertical tilt disappears and the growth shifts to higher levels. The perturbations were initially located around 90°W. Substantial downstream development produces a large impact of the perturbations close to Europe within 60 hours.

The analysis problem identified by the sensitivity calculations in this case has a major effect on the forecast performance over Europe from day 4 onwards. By day 5 the operational forecast missed an intense cyclogenesis over the Mediterranean ; consequently, over western Europe it has an upper-level ridge which has moved too far to the east (comparing Figs. 3 (a) and (b)). The modification of the analysis from the sensitivity calculations contributes to a substantial improvement of the upper-air flow pattern in the forecast, with the cut-off cyclone in the right position and a correct prediction of the ridge over Ireland and the UK (comparing Figs. 3 (a) and (c)).

Though most of the model integrations have been performed at a horizontal resolution of T106, similar results can be expected for the higher resolution of T213 used as the operational model version in 1994. For the case of 6 April the modification of the T213 analysis based on the T63 sensitivity pattern improves the high resolution forecast T213 even more than the T106 configuration of initial analysis and model formulation. A similar additional improvement was found in other sensitive cases running the high-resolution model.

In September 1993, a disturbance which could be identified as a weak remnant of hurricane Floyd developed explosively as an intense extratropical cyclone over the eastern Atlantic (top panel of Fig. 4 valid 12 UTC 12 September 1993) and affected the west coast of France and south-west England with gales and heavy rain. Five days before the explosive development, on 7 September, Floyd was a weak and decaying tropical depression 1200 km east of the coast of Florida. By 9 September, the weak disturbance was south of Nova Scotia and by 10 September it was over the west Atlantic (42°W, 46°N). Explosive development occurred during 11 and 12 September over the east Atlantic. As in some similar cases where air of tropical origin was involved in the development of a mid-latitude cyclone, the operational forecast performance was rather poor. The left hand column of Fig. 4 shows the operational forecast at different time ranges (day 2 from 10 September at top, ... day 6 from 6 September at bottom) all verifying on 12 September 1993. Even the short-range 2-day forecast completely underestimates the intensity of the cyclone. Forecasts at ranges of 2, 3, 4, 5 and 6 days failed in a similar way, by grossly underestimating the intensity of the low. The day 3 forecast did not have a low at all close to the west coast of France, whereas the 4, 5 and 6 day forecasts at least had a cyclonic flow pattern in the region, but not of the right intensity nor at the right place.

The forecast failures with mid-latitude disturbances of tropical origin suggest that errors in the diabatic forcing could be responsible for the underestimation of the cyclone development. Indeed, in the Floyd case, experimentation with a different convection scheme showed a sensitivity to diabatic forcing. The use of an adjustment scheme for convection improved these forecasts at medium range but not at short-range : there was no consistent improvement of the forecasts throughout the forecast ranges.

For this sequence of poor forecasts, the gradient of the day 2 forecast error has been used to modify the initial conditions at five different times ranging from two to six days before the development of the strong cyclone on 12 September. For the early forecasts up to 8 September, the main sensitivity was located over western parts of the USA.Only later, from 9 September, did the sensitivity coincide with the location of the surface low that developed into the storm three or four days later. It also seems that the perturbation derived from the sensitivity in the early forecasts improved not only the early low-level development, but also the upper-level flow, which provided the more favourable environment for the explosive development a few days later. All integrations from the modified analyses produce a deep cyclone on 12 September for all forecast ranges from day 2 to day 6 (right hand side panels of Fig. 4) and all forecasts reproduce the explosive development quite well during the same period on 11 and 12 September. Though the location and the intensity could still be improved, a forecast series like this would have given the forecaster a good basis for issuing the appropriate warnings of strong winds. In these cases it was beneficial to wait two days to produce an alternative forecast based on the sensitivity integration.

The « Floyd » experimentation again showed a marked sensitivity to initial conditions. There is also a sensitivity to the choice of convection scheme. However, the best forecast performance was obtained by combining the alternative convection scheme and the sensitivity perturbations.

For each day of April 1994 we produced the « control » forecast and the sensitivity integrations.

Vertical cross-sections of r.m.s. differences between the control and sensitivity runs, averaged over the latitude band 40°N to 65°N, are presented in Figs. 5 and 6 for temperature and vorticity. Panel (a) represents the initial perturbations, and the subsequent panels (b) to (d) show the evolution of the perturbations from day 1 to day 5. The initial perturbations exhibit maximum values between 400 and 700 hPa for temperature and between 500 and 850 hPa for vorticity ; the perturbations are thus mainly in the middle and lower troposphere. For idealized baroclinic instability (Rabier et al. 1992), the cyclogenesis was also found to be most sensitive to initial values around 700 hPa, which corresponded to the steering level. This fits well with the study of Farrell (1989) who relates the optimal excitation of unstable Charney modes to waves concentrated near the steering level. It is also consistent with the structure of the first singular vectors (Buizza and Palmer 1994). The evolution of these perturbations for the temperature field (Fig. 5), shows that the mid-troposphere structures initially located between 400 hPa and 700 hPa evolve rapidly to give maxima at two levels around 250 hPa and 500 hPa. The evolution of the vorticity perturbations (Fig. 6) shows that the region of largest amplitude moves upward rapidly in the first 24 hours from 850 hPa to between 400 hPa and 300 hPa. The perturbations located over north-east America grow much faster than any other local perturbations during the first two days, leading to large differences from the control run.

Operational performance in April 1994 showed typical day-to-day variations of forecast skill. The top panel of Fig. 7 shows the anomaly correlation for the T106 control experiments (dashed line) and the sensitivity experiments (solid line) for Europe and the bottom panel for the northern hemisphere. (Note the different scaling on the ordinate axis for these two panels). For Europe (Fig. 7 (a)) fairly good operational forecasts at the beginning of the month are followed by a complete failure on 6 April when the anomaly correlation drops to negative values. We have already shown in this section that this forecast was very sensitive to initial conditions and that the sensitivity run improved the day 5 forecast skill over Europe from -25 % to 85 %. The sensitivity perturbations do not improve only forecasts with low skill ; most forecasts from the modified analysis show an increase in forecast skill. An important feature of the sensitivity experiments is that their forecast skill is much more consistent throughout the month, suggesting that large day-to-day forecast

inconsistencies are closely related to analysis errors. A similar improved performance can be seen over the northern hemisphere (Fig. 7 (b))), where the control forecasts show three major periods of deterioration in skill with a drop of anomaly correlation close to 60 % whereas the sensitivity experiments follow a smoother line with anomaly correlations staying above 73 %. In other regions of the northern hemisphere, the sensitivity integration also usually performs better than the control forecast. Very few cases show a local deterioration.

# 4. KEY ANALYSIS ERRORS : MINIMIZATION OF FORECAST ERRORS

## 4.1 Optimization problem

In Klinker et al. (1998), the problem of finding relevant modifications to the analysis has been extended : let us now investigate a range of perturbations which might both represent part of the analysis error fairly well and improve the forecast substantially. These perturbations might no longer be « the most sensitive » perturbations, but will still be key analysis modifications if they grow reasonably fast and significantly affect the forecast performance.

A slightly different optimization problem will then be addressed : find a set of perturbation $\delta x$ which contribute to minimizing the forecast error squared norm

$$J(\delta x) = 1/2 \, || \, M(x^a)+\mathbf{M}.\delta x - x^{ref} \, ||^2$$

with respect to $\delta x$, where $M$ is the nonlinear model, $\mathbf{M}$ is the tangent-linear model, $x^a$ is the initial analysis, $x^{ref}$ is the verifying analysis, two days later.

In the minimization algorithm used to solve this optimization problem one iteration means one computation of J and of its gradient.

If one performed the full minimization of J:

$$M(x^a)+\mathbf{M}.\delta x - x^{ref} = 0$$

$$\delta x = -\mathbf{M}^{-1}(M(x^a)-x^{ref})$$

Assuming that $M(x^a)-x^{ref}=\mathbf{M}e_0$, $\delta x = -e_0$,

The perturbation is equal to the opposite of analysis error (such a method was used by Zupanski, 1995 ; Zou et al, 1998). Others have used pseudo-inverse methods to reach an estimate of analysis error, either by approximating $\mathbf{M}^{-1}$ by reversing in time $\mathbf{M}$ and changing the sign of the diffusion (Pu et al, 1998), or by inverting $\mathbf{M}$ in the subspace of singular vectors (Buizza et al, 1997).

In our study, ten steps of the minimization algorithm were performed in the 6 April 1994 case. Fig. 8, 9 and 10 (panels a), show the increments produced respectively after one, three and ten steps of minimization. Comparing panel a in Figs. 8, 9 and 10, one can notice that new increments appear at different locations, during the course of the minimization. The effect of the minimization is also to modify the amplitude of the increments. However, it does not drastically change the horizontal scales associated with these increments. After a few days of integration the three sets of perturbations evolve into a similar pattern. The decrease in the two-day forecast error as a function of the iteration number can be investigated. After a large decrease of 18 % in the cost function during the first iteration, the decrease slows down with further iterations to much smaller values and amounting to a total decrease of 51 % after ten iterations.

Performing a few steps of the minimization algorithm provides modifications to initial conditions that lead to additional improvement of forecast skill compared to integrations from the scaled gradient (see Fig. 11). It then seems beneficial to perform a few steps of the minimization algorithm in order to describe more accurately certain components of the analysis error.

### 4.2 Comparison with observations

The fit to the observational data is one criterion which can be used to discriminate between different perturbations to be added to the analysis. For any given perturbation $\delta x^a$ the goal is to compare the likelihood of two atmospheric states : the (initialized) analysis $\mathbf{x^a}$ and the modified analysis $\mathbf{x^a}+\delta\mathbf{x^a}$. The fit to the available data will be evaluated for atmospheric states of the form $\mathbf{x^a}+\alpha\,\delta\mathbf{x^a}$, which is for points in the direction of the perturbation $\delta\mathbf{x^a}$.

For any $\alpha$, the fit to the observations $\mathbf{y}$ is measured by the quantity

$$J_o(\alpha) = (H(x^a+\alpha\,\delta x^a)-y)^T R^{-1} (H(x^a+\alpha\,\delta x^a)-y)$$

with $H$ the observation operator, y the observation vector, R the observation error covariance matrix.

The "optimal" $\alpha_o$ is given by $\partial J_o/\partial\alpha = 0$.

The error variance in the estimation of $\alpha_o$ is $\sigma_o^2 = (\delta x^{aT}\mathbf{H}^T R^{-1}\mathbf{H}\delta x^a)^{-1}$, which depends both on $\delta x^a$ and the observations (number, accuracy).

The following table indicates, for each direction, the fit to the observations for $x^a$ ($\alpha$=0), $x^a+\alpha\,\delta x^a$ ($\alpha$=1), $\alpha_o$ and $J_o$.

| $\delta x^a$ | Iter 1 | Iter 3 | Iter 5 | Iter 10 |
|---|---|---|---|---|
| $J_o(0)$ | 41512 | 41512 | 41512 | 41512 |
| $J_o(1)$ | 41514 | 41399 | 41409 | 41734 |
| $\alpha_o$ | 0.48 | 1.02 | 0.61 | 0.39 |
| $\sigma_o$ | 0.14 | 0.10 | 0.05 | 0.03 |

One can see that 3 iterations moves the analysis significantly closer to the observations and $\alpha=1$ is very close to the optimal $\alpha_0$ (less than one standard-deviation away).

### 4.3 Limitations

The question one wants to answer is the following :

Why performing a large number of iterations in the minimization does not necessarily provide a better description of the analysis error ?

The main reason is that there is some uncertainty in the definition of the forecast error.

Both analysis and model errors ($\varepsilon$) enter this definition.

If the true error at time t is $e=\mathbf{M}e_0 + \varepsilon$ , one gets

$\delta x^a=-\mathbf{M}^{-1}(\mathbf{M}e_0 + \varepsilon)$

This implies that relevant information can only be extracted along the unstable directions of **M** (stable directions of $\mathbf{M}^{-1}$)

Another reason is that approximations in **M** are used in the minimization, which prevent finding the exact solution of the problem.

### 4.4 Statistics

As part of the operational suite at ECMWF the sensitivity of forecast errors to initial conditions is calculated on a daily basis. Since April 1995 the adjoint integrations to evaluate the gradient of the forecast errors with respect to the initial conditions have been extended by three steps of an iterative procedure which minimizes the day-2 forecast error as described in the previous sections.

Following the definition of sensitivity gradients in Rabier et al. (1996), the gradient of the day-2 forecast errors depends on forecast errors and on the stability of the flow through the adjoint operator $\mathbf{M}^*$. The Eady index as an approximation of the maximum growth rate of baroclinic waves provides a suitable measure for the baroclinicity of the flow, as shown for example by Hoskins and Valdes (1990). During the winter 1998/1999 the areas of maximum instability are found over the mid-latitude oceanic regions of the northern hemisphere (Fig. 12). In the Pacific both the maximum of instability of the flow and the maximum values of the scaled sensitivity gradient (Fig. 13) are located in the western Pacific where cyclones are mostly in their early developing phase. The close relation between stability and scaled sensitivity gradient shows that the latter provides a constrained estimate of the analysis error in the sense that it accounts only for the fastest growing errors. Sizeable analysis errors over the Pacific would also be expected from estimates in operational assimilation systems in which largest analysis uncertainties are assumed to be over oceans.

Indeed, the additional information on initial errors arising from three iterations (Fig. 14) has shifted the maximum of the implied analysis errors further to the east into the Central Pacific. From model integrations using the correction of the key analysis errors as perturbations and from control runs it is possible to compare the evolution of the key analysis errors with operational forecast errors.

These integrations are done on a daily basis with a model version of low horizontal resolution ($T_L$ 159) in order to support error tracking of the operational model. Within 12 hours key analysis errors evolve into structures that give a good indication of the geographical distribution of operational forecast errors well downstream of the main baroclinic zone over the East Pacific, suggesting that the perturbations found in the three iterations represent an important part of the analysis errors.

For a summer period (June 1995) and a winter period (February 1996) two sets of integrations were run. For each period, one set from the operational analysis (control runs) and a second set from the analysis with perturbations superimposed that compensate the key analysis errors (perturbed runs).

During the model integration the evolution by key analysis errors affects forecast errors over most area of the northern hemisphere. At the optimization time of two days the compensation of key analysis errors reduces the r.m.s. errors by between 30 and 40 % in the major storm track regions in the middle latitudes of the northern hemisphere.

Over the full northern hemisphere north of 20°N the evolution of key analysis errors (Fig. 15 (a), dotted line) shows a non-linear increase in the first two days of integration time, during which the forecast errors of the control runs (solid line) are reduced by 2 m at day-1 and 7.5 m by day-2 in the perturbed runs (dashed line). Beyond day-2 the benefit of reducing errors in the initial conditions remains almost constant.

In the summer month of June 1995 the error growth of the control integrations is noticeably smaller than in February 1996 (Fig. 15 (b)). A corresponding smaller sensitivity gradient in the summer can easily be explained by an atmospheric structure that is less baroclinically unstable in summer than in winter. However, the key analysis errors are not very much different in the two different months. In effect the time evolution of the key analysis errors in summer and winter seems to be almost identical, with only a slightly smaller non-linear increase in the short range forecast (day-1 to day-2) and towards the end of the ten day integration period. It is therefore not surprising that key analysis errors contribute equally to forecast errors in absolute terms in summer and winter, at least up to day-5. The decreasing influence of key analysis errors after day-6 in the summer might be due to the increasing importance of model errors from the parametrization of sub-grid processes.

A useful measure of consistency in subsequent forecasts is to calculate the r.m.s. differences between consecutive forecasts. Fig. 15 shows the result for the control integrations (thin line) and integrations where the key analysis errors have been eliminated (thin dashed line). It is clear from this that the reduction of analysis errors using three iterations in the minimization of day-2 forecast errors has a beneficial effect on the consistency of subsequent forecasts. In r.m.s. terms the improvement of the consistency is large compared to the reduction of the forecast errors itself, suggesting that the average improvement of forecast skill has been achieved by improving the worst cases the most.

One might be tempted to interpret the difference between the r.m.s. errors and the consistency for the two sets of integrations as a measure for a potential model improvement as suggested by Lorenz (1982). This would suggest that the reduction of key analysis errors would also increase the model improvement potential as the difference between the r.m.s. errors and the r.m.s. of the consistency is clearly larger for the integrations with compensated key analysis errors. An important change in the ECMWF forecasting system occured in November 1997 with the change from a three-dimensional to a four-dimensional data assimilation (Rabier et al., 1997). This resulted in a significant improvement of forecast performance at all ranges. Key analysis errors were computed for the same period for both old and new systems. A reduction of key analysis errors was noticed with the change to four-dimensional data assimilation, consistent with the general improvement caused by the change.

## 5. REAL-TIME DIAGNOSTIC OF FORECAST BEHAVIOUR

The strategy developed at Météo-France consists in using the adjoint tool to provide guidance to forecasters and possibly to investigate alternatives to the reference forecast. Because of this operational constraint, the objective function has to be a function of the forecast variables only and not of the forecast error. Because of this choice, the information provided by the adjoint tool indicates areas where errors are likely to grow rapidly towards a dramatic change in the objective function but not necessarily on locations where errors actually occurred.

To produce an alternative analysis and a subsequent forecast it is then necessary to bring new information together with the sensitivity information. It is then important to add as much information as possible from observational sets in order to detect and possibly correct an initial error inside the sensitive areas.

The initial correction to an analysis might control the initial error on the most unstable directions i., e., the first unstable plan (Bergot et al. 1999). The initial error is not known on this procedure but could be approximated by the calculation of the singular vectors (the error is approximated by a perturbation which will grow most rapidly over a time period and for a given norm) or by the calculation of sensitivity fields (the error is approximated by a perturbation which will maximise a change on the objective function of the forecast variables).

The idea is to modify the initial conditions with the same structure as sensitivity vectors but with the constraint that inside the sensitive area (the geographic area where the gradient fields are not equal or close to zero) the distance between the new initial state and the observations available is minimal. An alternative forecast can then be produced based on this perturbed analysis : $x^a+\alpha\ \delta x^a$ with $\alpha$ optimized.

The application case chosen here is one when a severe storm occurred. The unstable aspect of this case and the likely contribution of initial conditions uncertainty made it a good candidate to test the method.

The so-called Christmas storm hit the British Isles on the day and night of the 24 of December 1997. It was a severe storm which caused serious damages. It is also well-known because it is an important failure case for forecasts produced by many operational centres at short ranges. The surprising aspect of the forecast performance is that some long range numerical forecasts (96 hours forecasts) were able to predict the storm quite well and then this storm is lost at shorter ranges.

The fact that the storm is reasonably well forecast in the medium-range is a good indication that both the physics and the dynamics of models are sufficient to resolve the relevant processes and therefore a sensitivity study is fully relevant. The model which is referred to from now on is the ARPEGE Météo-France operational model at this time : 3 dimensional variational assimilation scheme, triangular spectral truncation T149 with a variable mesh and a stretching factor of 3.5 (meaning that the resolution is equivalent to a T520 near the pole of interest which is located inside France and equivalent to a T42 at the opposite pole) (Courtier et al. 1991). The last good ARPEGE forecast is the one based on the analysis of the 971221 at 00 UTC (84 hours forecasts). Then the model is no longer predicting the storm.

The study is focussing on the forecast based on the 971223 at 00 UTC analysis. An example of the mishandling of the storm by this run is given on Fig. 16 by a comparison with the long range forecast (right panels in Fig. 16) which is the last operational ARPEGE good forecast of this storm. This forecast is not the worst one : it is at least predicting the storm, but with an important delay and underestimation. The objective function is computed inside the $\Omega$ area at the location of a ridge on the 36 hour forecast (see Fig. 16 (c)).

The gradient fields give a sensitive area on the 971223 at 00 UTC located between 45 N-30 N and 50 W-30 W. The gradients are pointing out the phase delay that the forecast based on 971223 00 UTC will amplify in the later stages of the forecast.

Several alternative forecasts to the operational one are processed. They are done with the observations grouped into different sets such as : synop (land and ship) surface observations, airep high level observations by aircrafts, buoys sea level observations, satob (geostationnary satellite imagery derived wind) vertical profiles from high levels totop of clouds, and temps (radiosondes) vertical profiles. The first application of the method is to look at the sign that the minimisation process gives for each observation type. The sign of the tuned parameter $\alpha$ is always negative. This means that the observations inside the sensitive area (located between 50 N-28 N and 50 W-25 W) are anticipating a deepening inside the $\Omega$ area or in other words, that the 36 hour forecast inside the $\Omega$ area is not deep enough according to observations located inside the sensitive area at analysis time.

The amplitude of the tuned parameter $\alpha$ is different depending on the type of observation sets. There are two distinct groups : one which is formed with the synop, buoys and airep sets, and the other one with a weaker amplitude of the $\alpha$ parameter which is made of the satob and temp sets. The weak amplitude of the temp experiment is due to the fact that there is only one vertical profile and it is also not located in a place where the gradient values are strong (see Fig. 17 (b)). On the contrary, the satob observations are covering entirely the sensitive area (see Fig. 17 (a)). The explanation of the weak amplitude of the satob-tuned $\alpha$ parameter could be that because of the large number of observations, the analysis is already at a minimum distance from these observations. And so, the process of pulling the analysis towards observations within the gradient structure is inefficient. It could also be due to the fact that the satob observations are vertically located at the top of the cloud which is often relatively high and especially at the place where the gradients signal is very weak. For this group, the amplitude of the perturbation is too small to be efficient (see Fig. 17 (a) and (b)). For the other group (synop, buoys, airep), the observations are more sparse. And even if they are quite a few (like for the buoys experiment), they are located in an area of strong gradient values. For those cases, the amplitude of the perturbation is large enough to be efficient : the perturbed forecast is then able to predict the storm (see Fig. 17 (c) and 17 (d) and (e)). The perturbation is even sometimes overdoing it, but the process of closeness of analysis towards observations within gradient structure is enlarging the impact of the observations when they are not so numerous. When looking at the different forecasts on Fig. 17, one can estimate an interval of values including the intrinsic value of parameter $\alpha$ : between -10 and -30.

One can calculate the variance of the error made on the determination of the parameter $\alpha$ .

The expression of this variance means that the error done on the determination of the parameter $\alpha$ is in proportion with the matrix R. Then one can best trust $\alpha$ values which are computed with small values of $\sigma_o$ : standard deviation of observational error. This is the case for the synop observations, but not for the satob ones. The satob observation type is rather inaccurate. It is an estimation of wind done with complex algorithms taking into account the displacement of clouds, the altitude of this displacement is estimated from temperature values with high $\sigma_o$ .

## 6. CONCLUSION

In this paper, we have discussed various applications of the adjoint method to sensitivity analysis, and in particular to the diagnostic of forecasting system performance.

After revisiting the mathematical basis of the adjoint method, main results obtained by Rabier et al. (1996) and Klinker et al. (1998) about the sensitivity of forecast errors to initial conditions were presented. These can be summarized by the following points :

- Gradient-based modifications of the analysis peak in the middle to lower troposphere.
- Gradient-based modifications of the analysis are small-scaled structures tilted in the vertical, well within error bars.
- Sensitivity integrations substantially improve the forecast, well beyond the two-day range.
- Sensitivity integrations can have a prognostic value in specific case (spell of bad forecasts).

- Key analysis errors obtained by 3 iterations of the minimization of forecast error are less constrained by instability of the atmosphere than sensitivity fields (geographical distribution, seasonal amplitude): they highlight errors which are both fast-growing and in data-sparse areas.
- Averaged local improvement reaches 40% locally at day 2.
- They lead to significant improvement in the medium-range.
- These key analysis errors can be used to evaluate forecasting system changes.

As a summary, these key analysis errors are reliable estimates of the part of the analysis that is largely responsible for the short-range forecast errors.

In a real-time application of the adjoint method, Hello et al. (1999) impose a « sensitive structure » to an analysis correction. The tuning of the perturbation amplitude is obtained by reducing the distance to the observations at the locations where the sensitive structure is of significant amplitude.

It is also possible to tune both initial conditions and model parameters using the adjoint model. Relevant references are given below, for various applications :

- Minimization of the distance to observations to get model error (Derber, 1989), or model parameters (Rinne and Järvinen, 1993).
- Minimization of the distance of forecast to observations to get model error and initial conditions (Zupanski, 1997).
- Minimization of the distance of forecast to observations to get model parameters and initial conditions (Zhu and Navon, 1999).

The adjoint model can also be applied as a real-time tool for a strategy for adaptive observations (Gelaro et al., 1999 ; Pu et al. 1998 ; Bergot et al., 1999).

As a general conclusion, although developing the adjoint model of a numerical forecasting model is time-consuming, the availability of such a tool allows to investigate a wide range of applications, including data assimilation, predictability and diagnostics. For the diagnostic side of applications, the sensitivity to initial conditions has proved useful to investigate the performance of the forecasting system.

Another potential application could be to use these key analysis error statistics as a tool to help redesign the global observing-system.

## 7. REFERENCES

Arbogast P., 1998 : Sensitivity to potential vorticity. Quart. Jour. Roy. Meteor. Soc., vol. 124, pp. 1605-1615.

Bergot T., Hello G., Joly A. and Malardel S., 1999 : Adaptive observations : a feasibility study. Mon. Wea. Rev., vol. 127, pp. 743-765.

Buizza R. and Palmer T.N., 1994 : The Singular-Vector structure of the Atmospheric General Circulation. Jour. Atmos. Sci., vol. 52, n° 9, pp. 1434-1456.

Buizza R., Gelaro R., Molteni F. and Palmer T.N., 1997 : The impact of increased resolution on predictability studies with singular vectors. Quart. Jour. Roy. Meteor. Soc., vol. 123, pp. 1007-1033.

Courtier P., Freydier C., Geleyn J.F., Rabier F. and Rochas M., 1991 : The ARPEGE project at Météo-France. ECMWF Seminar Proceedings, Sept. 1991, pp. 193-231.

Errico R.M. and Vukicevic T., 1992 : Sensitivity analysis using an adjoint of the PSU/NCAR mesoscale model. Mon. Wea. Rev., vol. 120, pp. 1644-1660.

Errico R.M., Vukicevic T. and Reader K., 1993 : Comparison of initial and lateral boundary condition sensitivity for a limited-area model. Tellus, vol. 45A, pp. 539-557.

Farrell B.F., 1989 : Optimal excitation of baroclinic waves. Jour. Atmos. Sci., vol. 46, pp. 1193-1206.

Farrell B.F., 1990 : Small error dynamics and the predictability of atmospheric flows. Jour. Atmos. Sci., vol. 47, pp. 2409-2416.

Gelaro R., Langland R.H., Rohaly G.D. and Rosmond T.E., 1999 : The use of adjoint methods for adaptive observations. Proceedings of the ECMWF Workshop on predictability, 20-22 October 1997, pp. 153-183.

Hall M.C.G., Cacuci D. and Schlesinger M.R., 1982 : Sensitivity analysis of a radiative-convective model by the adjoint method. Jour. Atmos. Sci., vol. 39, pp. 2038-2050.

Hall M.C.G., 1986 : Application of adjoint sensitivity theory to an atmospheric general circulation model. Jour. Atmos. Sci., vol. 43, pp. 2644-2651.

Hello G., Lalaurette F. and Thépaut J.N., 1999 : Combined use of sensitivity information and observations to improve meteorological forecast : a feasibility study applied to the « Christmas Storm ». Accepted for publication in Quart. Jour. Roy. Meteor. Soc.

Horanyi A. and Joly A., 1996 : Some aspects of the sensitivity of idealized frontal waves. Beitr. Phys. Atmos., vol. 69, pp. 517-533.

Joly A., 1995 : The stability of steady fronts and the adjoint method : Non-modal frontal waves. Jour. Atmos. Sci., vol. 52, pp. 3082-3108.

Klinker E., Rabier F. and Gelaro R., 1998 : Estimation of key analysis error using the adjoint technique. Quart. Jour. Roy. Meteor. Soc., vol. 124, pp. 1909-1933.

Langland R.H., Elsberry R.L. and Errico R.M., 1995 : Evaluation of physical processes in an idealized extratropical cyclone using adjoint sensitivity. Quart. Jour. Roy. Meteor. Soc., vol. 121, pp. 1349-1386.

Le Dimet F.X. and Talagrand O., 1986 : Variational algorithms for analysis and assimilation of meteorological observations. Tellus, vol. 38A, pp. 97-110.

Lorenz E.N., 1982 : Atmospheric predictability experiments with a large numerical model. Tellus, vol. 34, pp. 505-513.

Marais C. and Musson-Genon L., 1992 : Forecasting the surface weather elements with a local dynamical-adaptation method using a variational technique. Mon. Wea. Rev., vol. 120, pp. 1035-1049.

Oortwijn J. and Barkmeijer J., 1995 : Perturbations that optimally trigger weather regimes. Jour. Atmos. Sci., vol. 52, pp. 3932-3944.

Pu Z.X., Lord S. and Kalnay E., 1998 : Forecast sensitivity with dropwindsonde data and targeted observations. Tellus, vol. 50A, pp. 391-410.

Rabier F., Courtier P. and Talagrand O., 1992 : An application of adjoint models to sensitivity analysis. Beitr. Phys. Atmos., vol. 65, pp. 177-192.

Rabier F., Klinker E., Courtier P. and Hollingsworth A., 1996 : Sensitivity of forecast errors to initial conditions. Quart. Jour. Roy. Meteor. Soc., vol. 122, pp. 121-150.

Rabier F., J.F. Mahfouf, M. Fisher, H. Järvinen, A. Simmons, E. Andersson, F. Bouttier, P. Courtier, M. Hamrud, J. Haseler, A. Hollingsworth, L. Isaksen, E. Klinker, S. Saarinen, C. Temperton, J.N. Thépaut, P. Unden and D. Vasiljevic, 1997 : Recent experimentation on 4D-Var and first results from a Simplified Kalman Filter. ECMWF Research Department Technical Memorandum, n° 240, Nov. 1997.

Zou X., Kuo Y.H. and Low-Nam S., 1998 : Medium-range prediction of an extratropical Oceanic cyclone : Impact of initial state. Mon. Wea. Rev., vol. 126, pp. 2737-2763.

Zupanski M., 1995 : An iterative approximation to the sensitivity in calculus of variations. Mon. Wea. Rev., vol. 123, pp. 3590-3604.

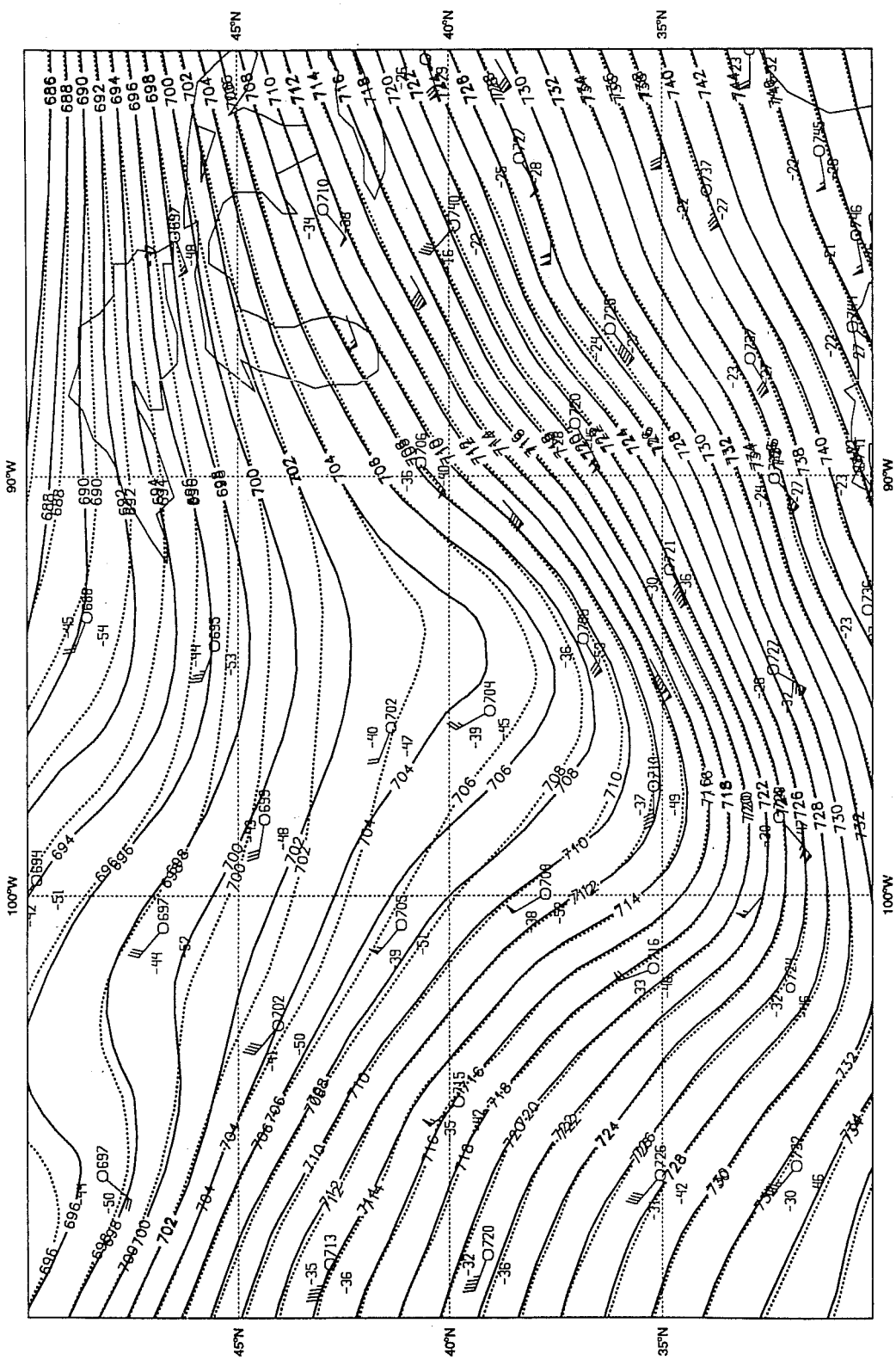


Figure 1. Operational initialized height analysis (dotted contours), and analysis modified by a perturbation proportional to the gradient of the day-two forecast error (solid contours) and observations at 400 hPa for 6 April 1994.

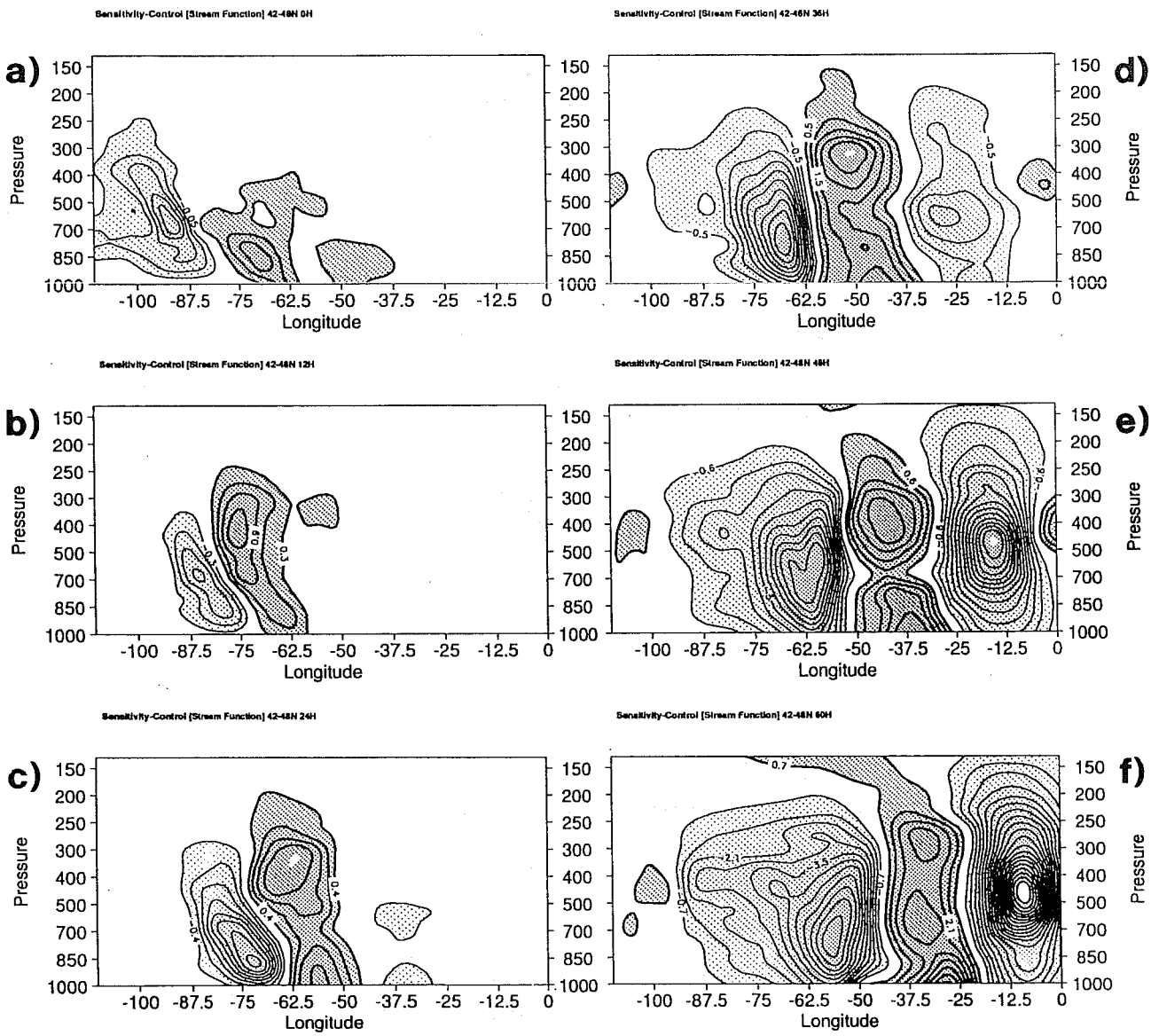


Figure 2. Vertical west-east cross-sections of the sensitivity perturbations following the latitude of the maximum perturbation amplitude for range in hours 0, 12, 24, 36, 48 and 60. The quantity shown is the streamfunction perturbation for the forecast from 6 April 1994. Unit : $10^6 m^2 s^{-1}$. Contour intervals are (a) 0.05, (b) 0.3, (c) 0.4, (d) 0.5, (e) 0.6 and (f) 0.7.

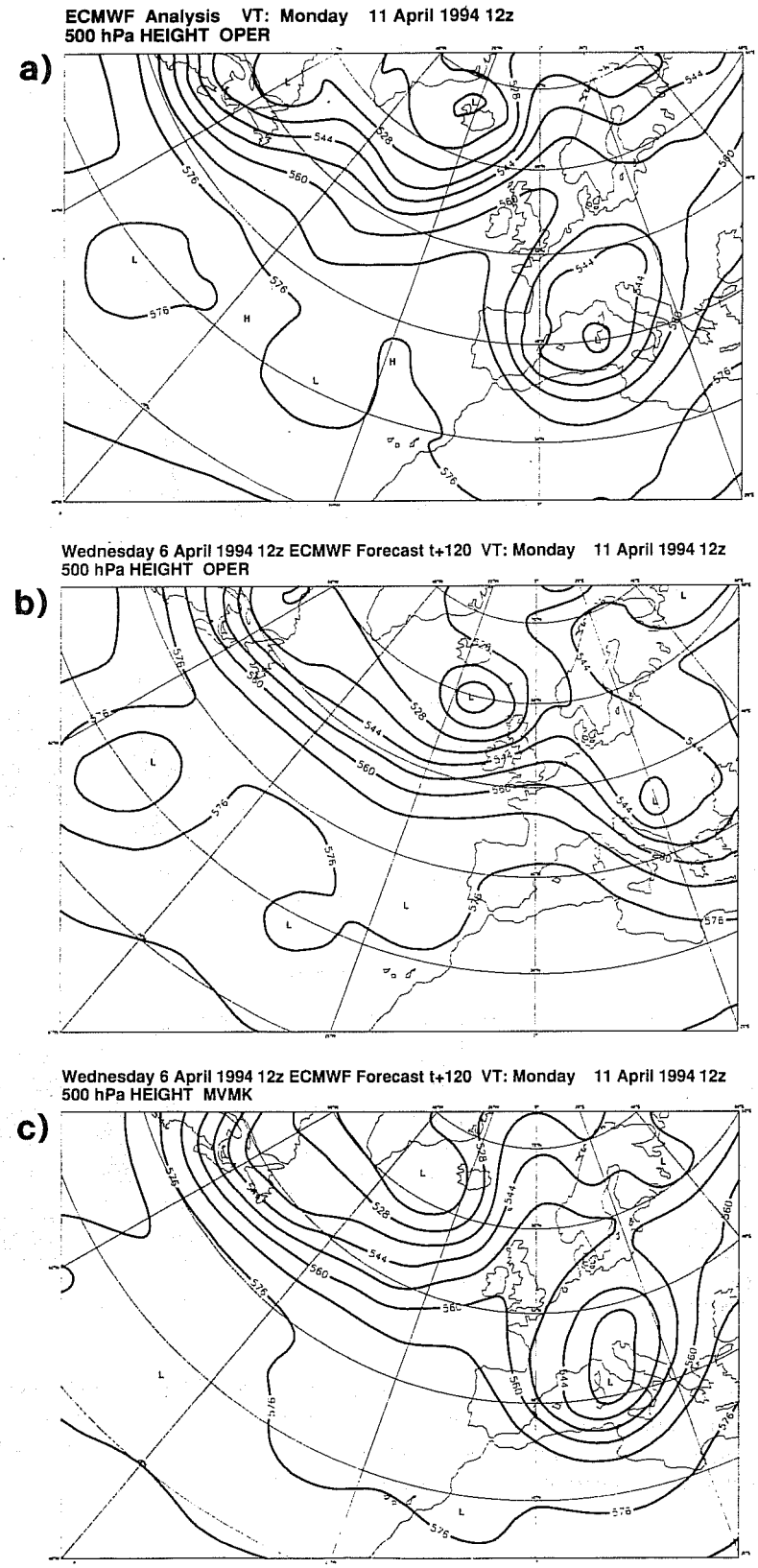


Figure 3. Geopotential of the 500 hPa surface for 11 April 1994 : (a) verifying analysis ; (b) operational forecast and (c) sensitivity integration. (Forecast range 120 hours). Units : tens of gpm.

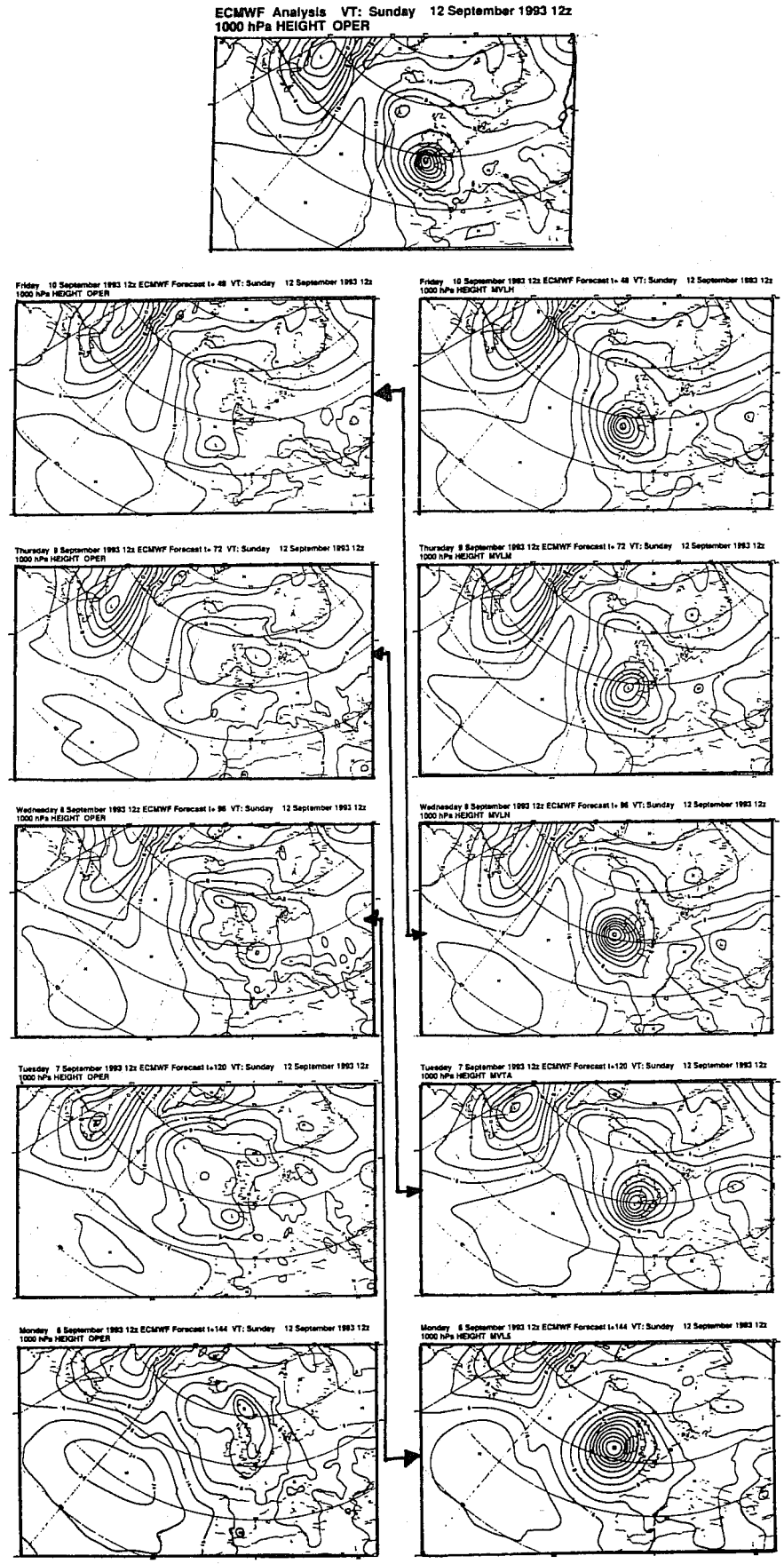


Figure 4. Geopotential of the 500 hPa surface for 12 UTC 12 September 1993 : (top panel) verifying analysis ; (left column) operational forecast and (right column) sensitivity integration. (Forecast ranges as shown on left). Units : tens of gpm. The arrows indicate which integrations had access to the same information.

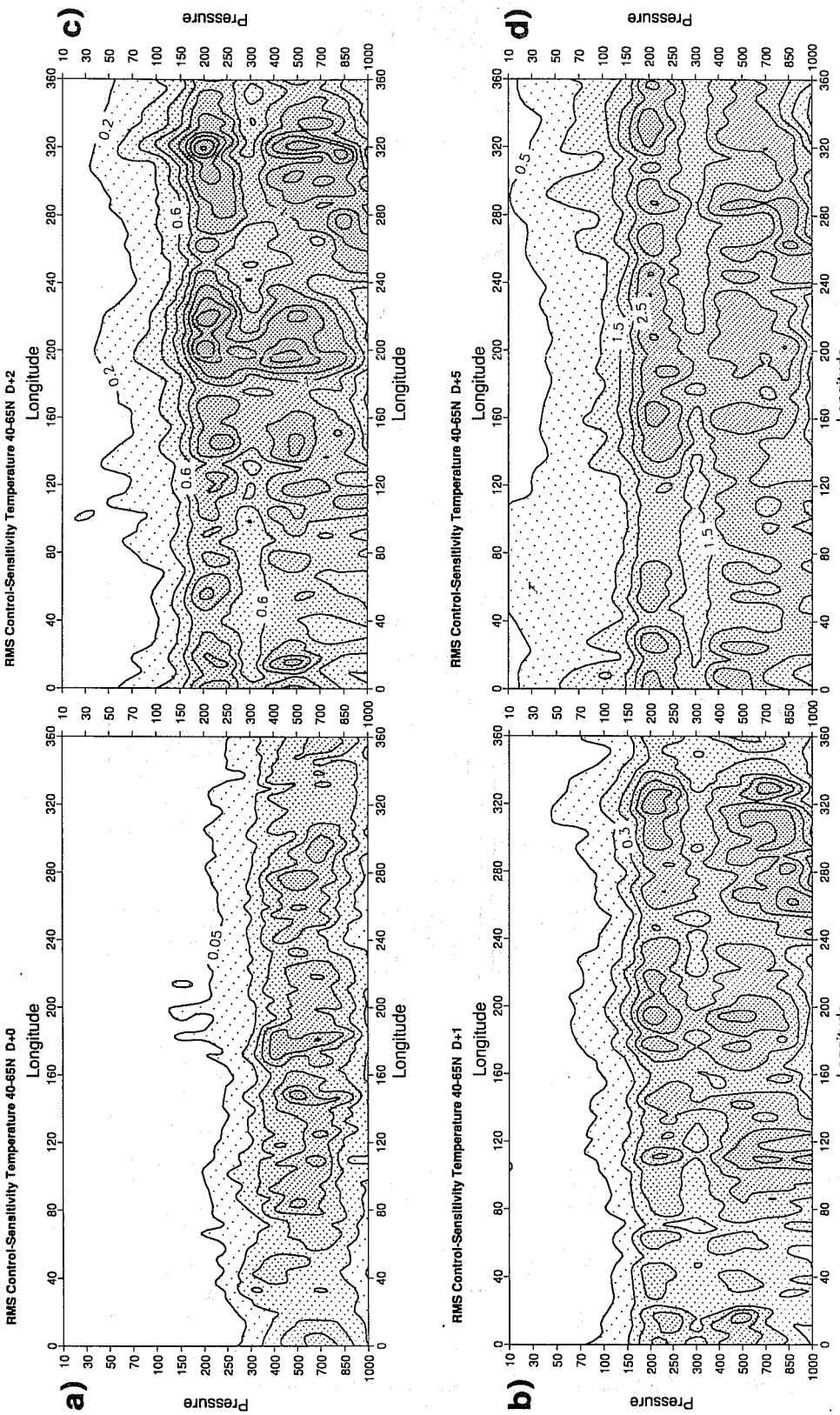


Figure 5. Vertical west-east cross-sections over the latitude band 40°N-65°N of root mean squares of sensitivity perturbations in April 1994 for temperature at (a) the initial time, and at forecast ranges of (b) 1 day, (c) 2 days and (d) 5 days. Unit : K. Contour intervals are (a) 0.05, (b) 0.1, (c) 0.2 and (d) 0.5.

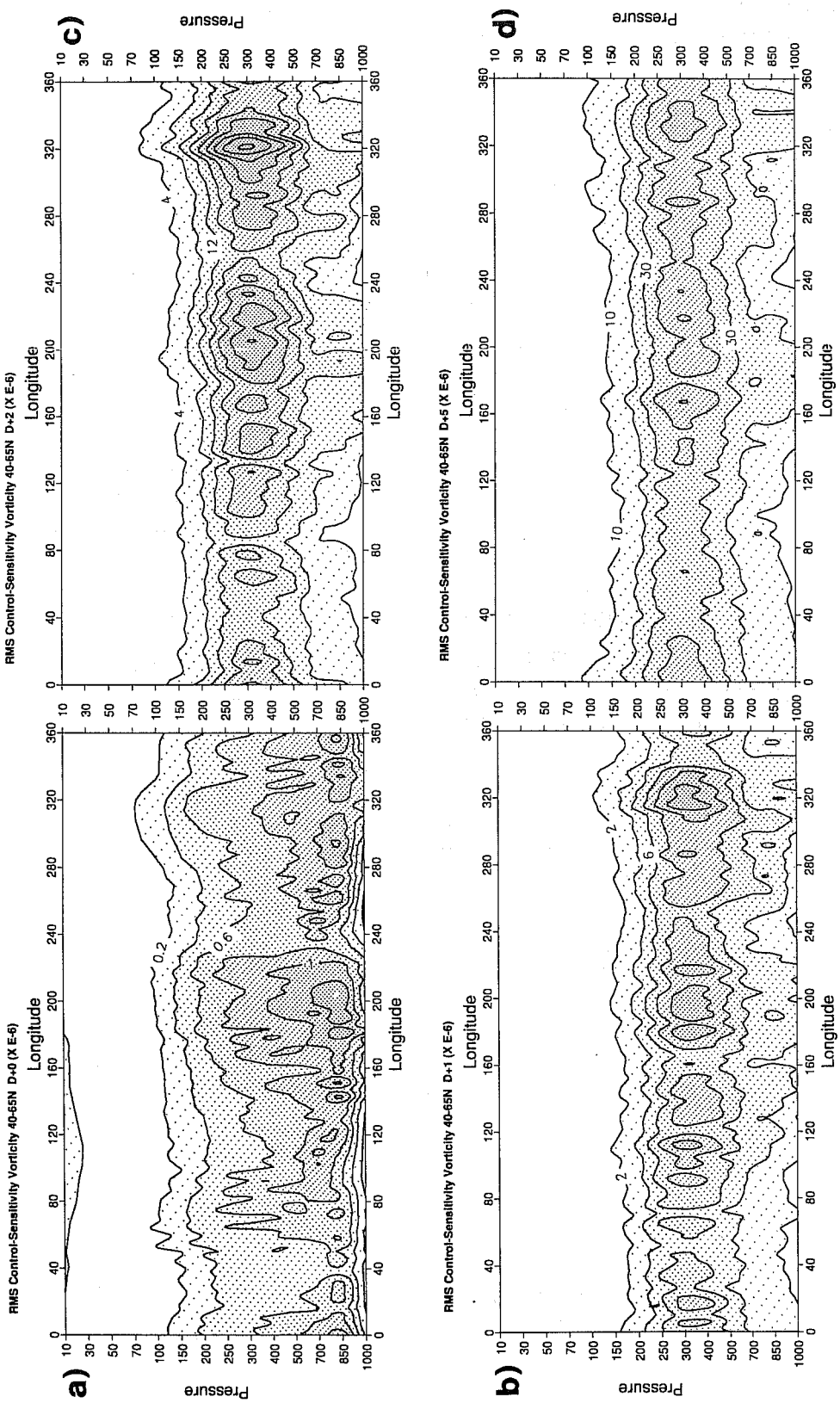


Figure 6. Vertical west-east cross-sections over the latitude band 40°N-65°N of root mean squares of sensitivity perturbations in April 1994 for vorticity at (a) the initial time and at forecast ranges of (b) 1 day, (c) 2 days and (d) 5 days. Unit : $10^{-6}s^{-1}$. Contour intervals are (a) 0.2, (b) 2, (c) 4 and (d) 10.

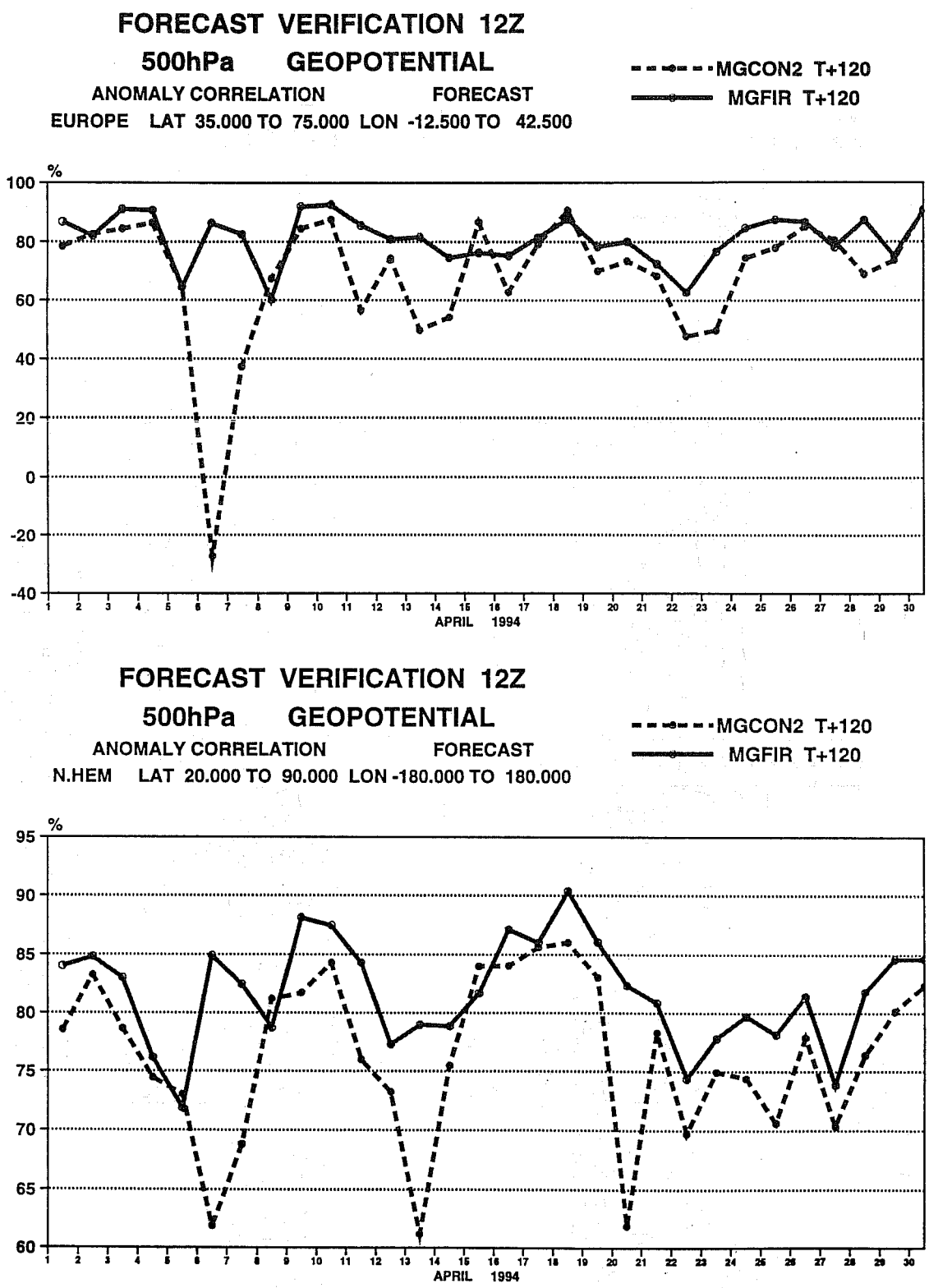


Figure 7. Time series of day 5 anomaly correlations for (a) Europe (35°N-75°N, 12.5°W-42.5°E) and (b) the northern hemisphere (20°N-90°N). Control forecasts, dashed line ; sensitivity integrations, solid line. Note the different scales of percentage correlation.

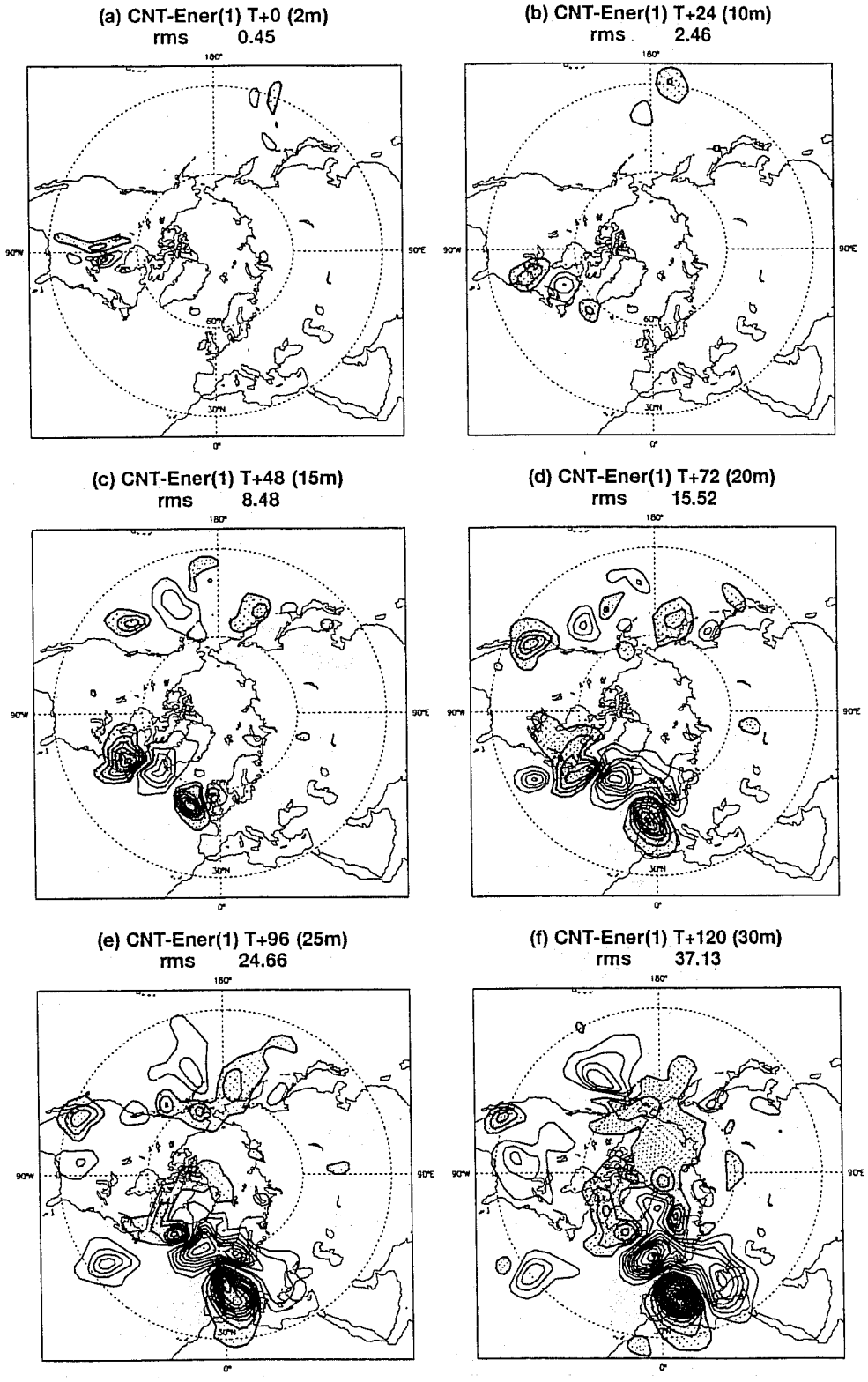


Figure 8. Difference between the sensitivity integration started from the analysis perturbed by as scaled gradient with respect to energy inner-product and the control forecast ranges day 0, day 1, ..., day 5 for 6 April 1994. Units : gpm. Note the different contour intervals used in the panels (shown is brackets) : day 0, 2 m ; day 1, 10 m ; day 2, 20 m ; day 3, 45 m ; day 4, 60 m ; day 5, 75 m. R.m.s. value for each map shown in metres.

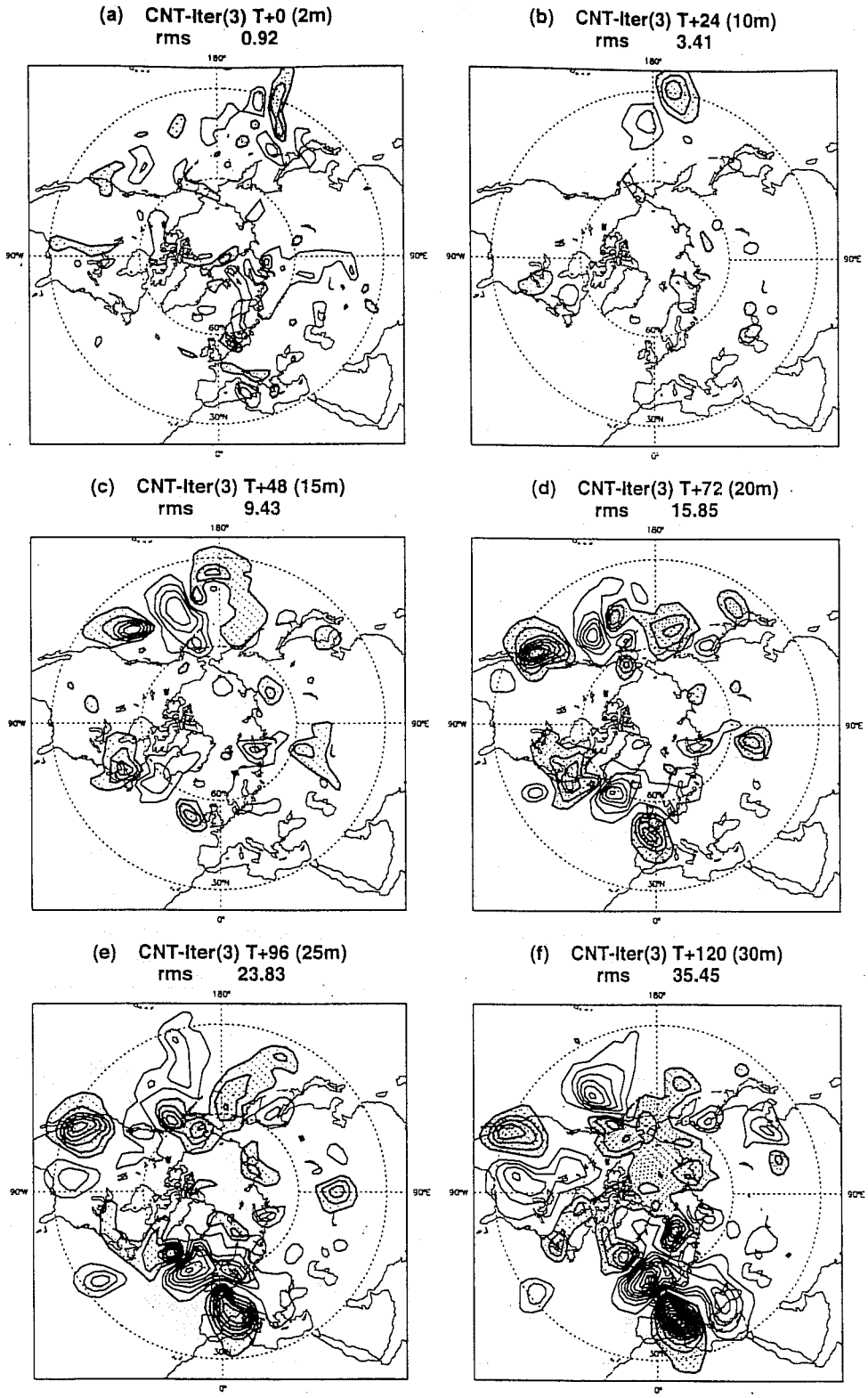


Figure 9. Difference between the sensitivity integration started from the analysis perturbed by the increment based on 3 iterations and the control forecast for forecast ranges day 0, day 1, ..., day 5 for 6 April 1994. Units : gpm. Note the different contour intervals used in the panels (shown in brackets) : day 0, 2 m ; day 1, 10 m ; day 2, 20 m ; day 3, 45 m ; day 4, 60 m ; day 5, 75 m. R.m.s. value for each map shown in metres.

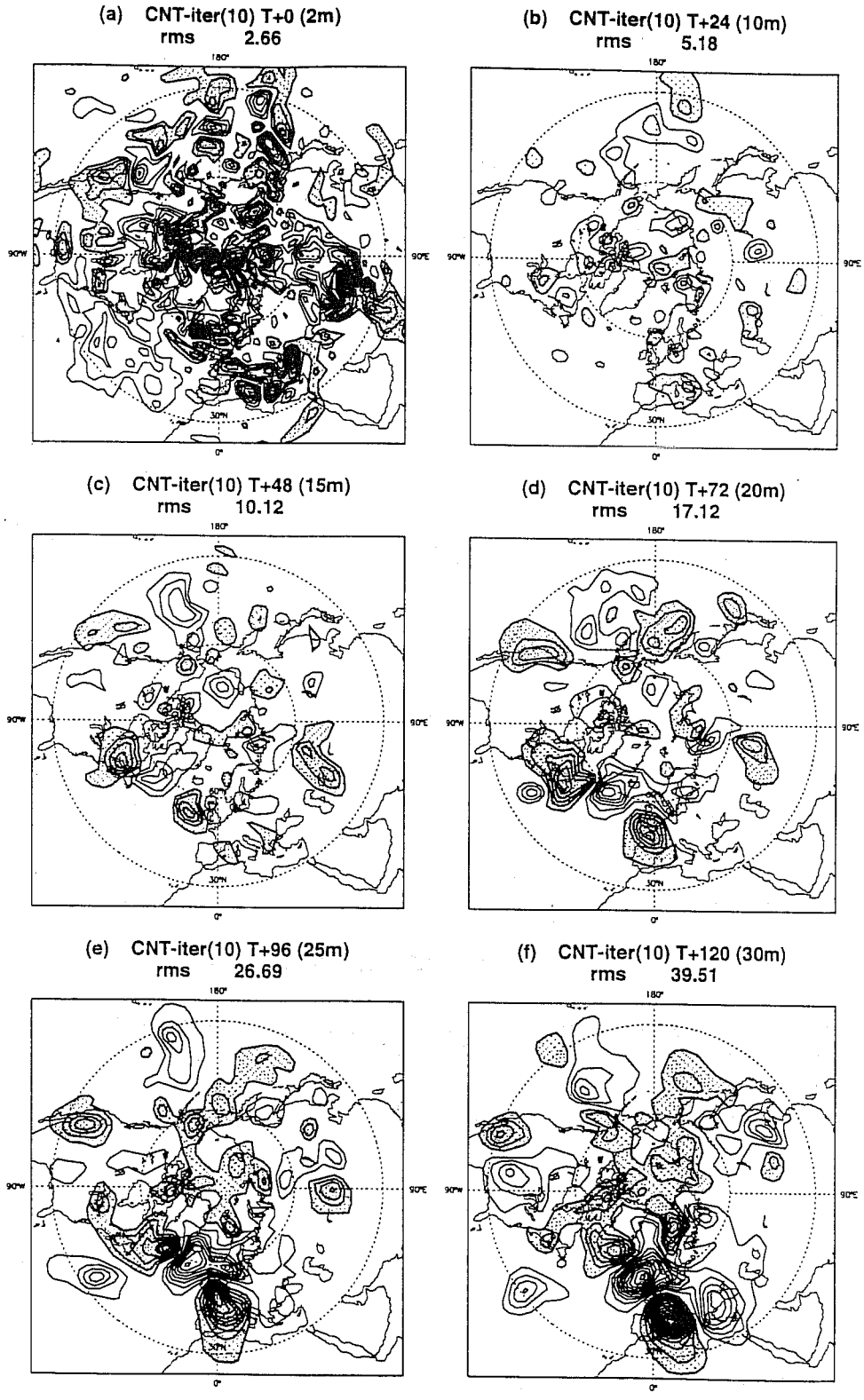


Figure 10. Difference between the sensitivity integration started from the analysis perturbed by the increment based on 10 iterations and the control forecast for forecast ranges day 0, day 1, ..., day 5 for 6 April 1994. Units : gpm. Note the different contour intervals used in the panels (shown in brackets) : day 1, 10 m ; day 2, 20 m ; day 3, 45 m ; day 4, 60 m ; day 5, 75 m. For day 0 contours are drawn at +/-2 m, +/-6 m, +/-10 .... R.m.s. value for each map shown in metres.

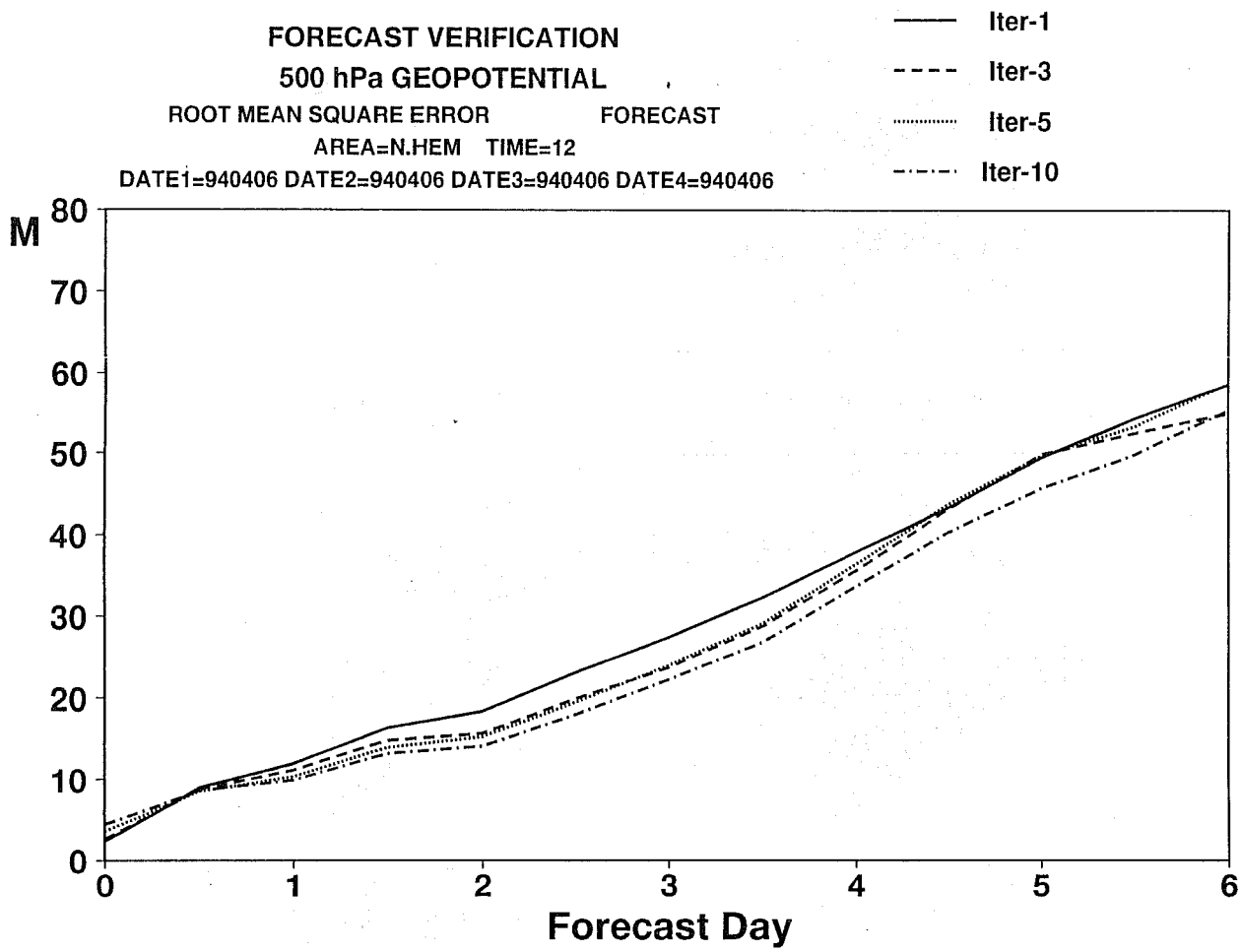


Figure 11. Forecast scores for 6 April 1994 (r.m.s. error for northern hemisphere). Scores are shown for the sensitivity integrations based on the first iteration of the minimization (equivalent to energy-based scaled gradient, solid line) the third iteration (dashed line), the fifth iteration (dotted line) and the tenth iteration (dashed-dotted line).

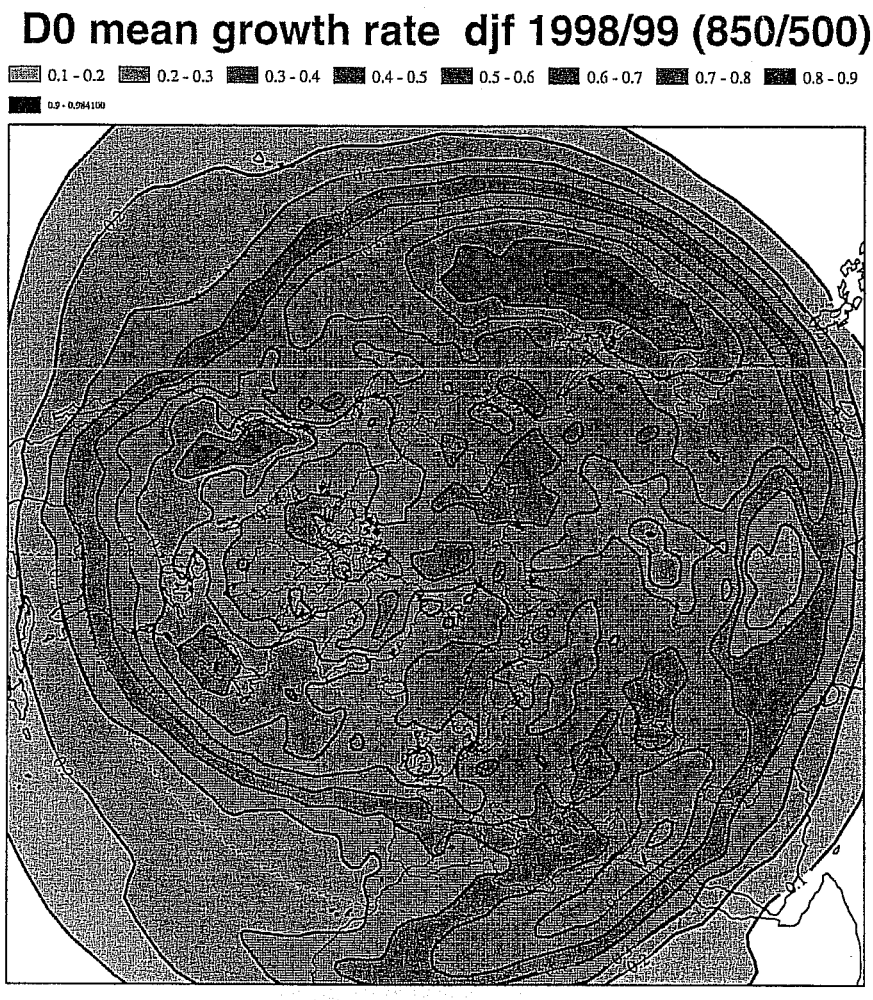


Figure 12. Eady index for winter 1998/1999.

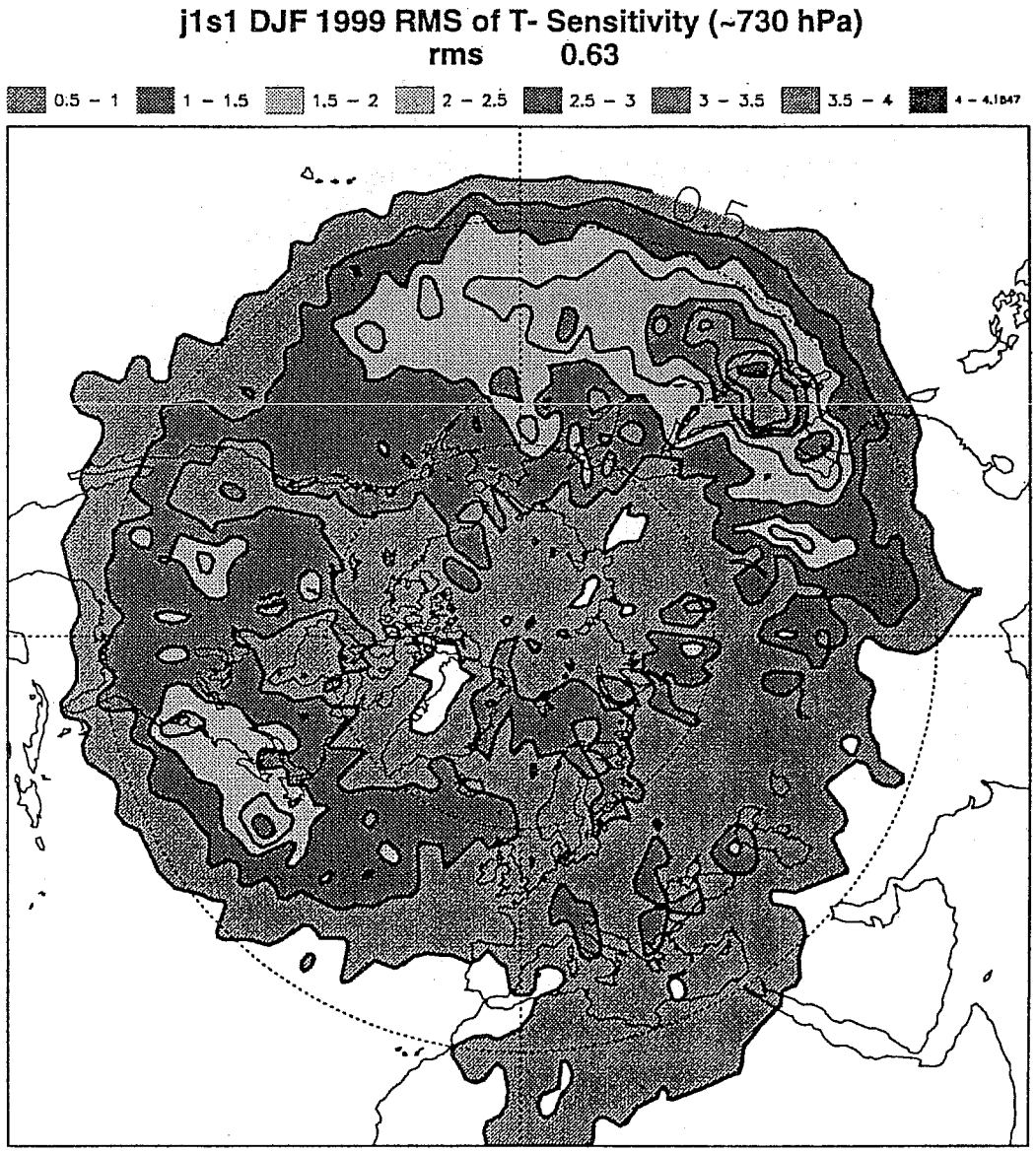


Figure 13. R.m.s. values of optimally scaled gradient of day-2 forecast errors with respect to initial temperature at 730 hPa for winter 1998/1999. Contour interval : 0.5, 1, ..., 3 K.

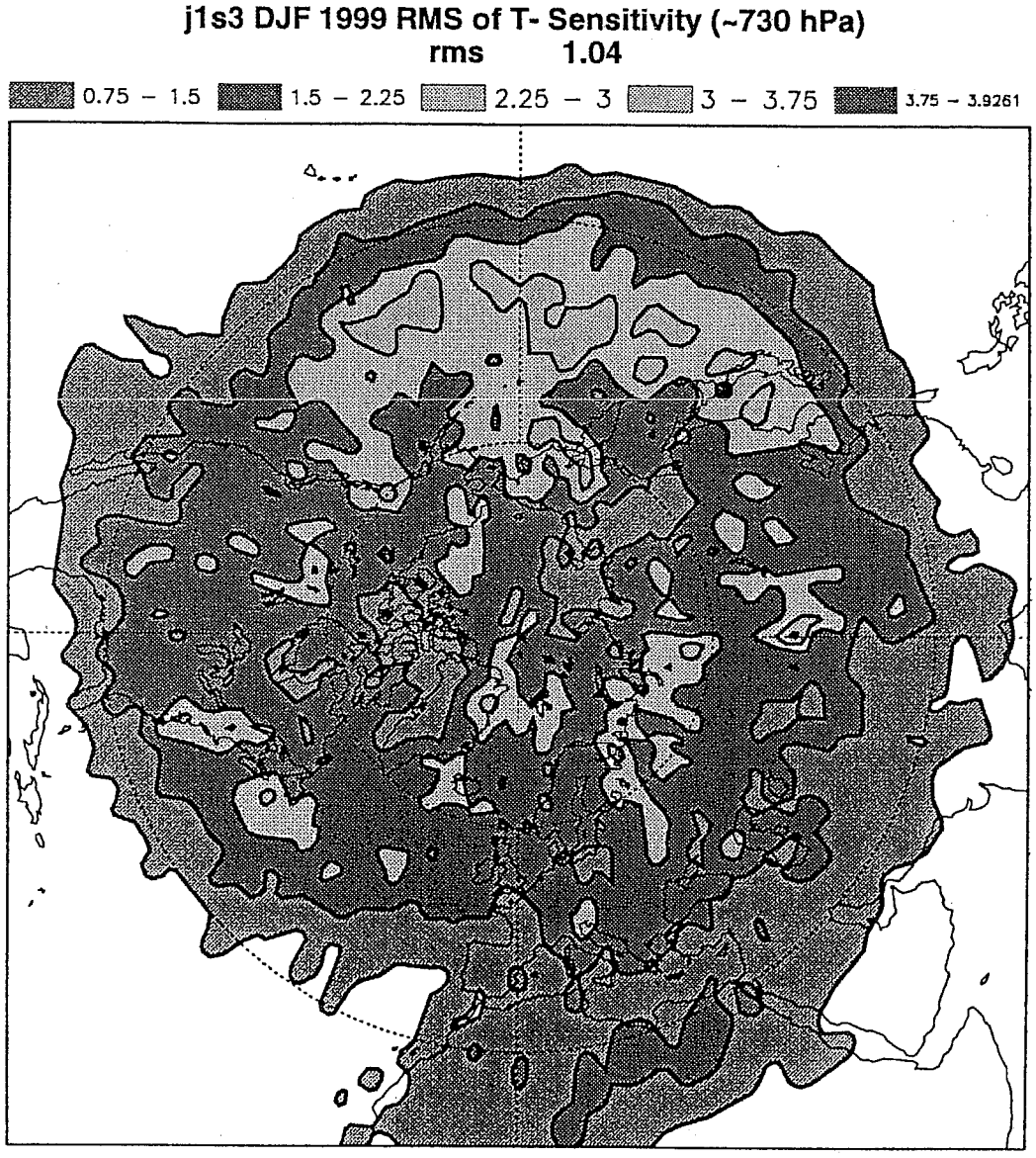


Figure 14. R.m.s. values of key analysis errors of temperature for 730 hPa for winter 1998/1999. Contour interval : 0.75, 1.5, ....3.75 K.

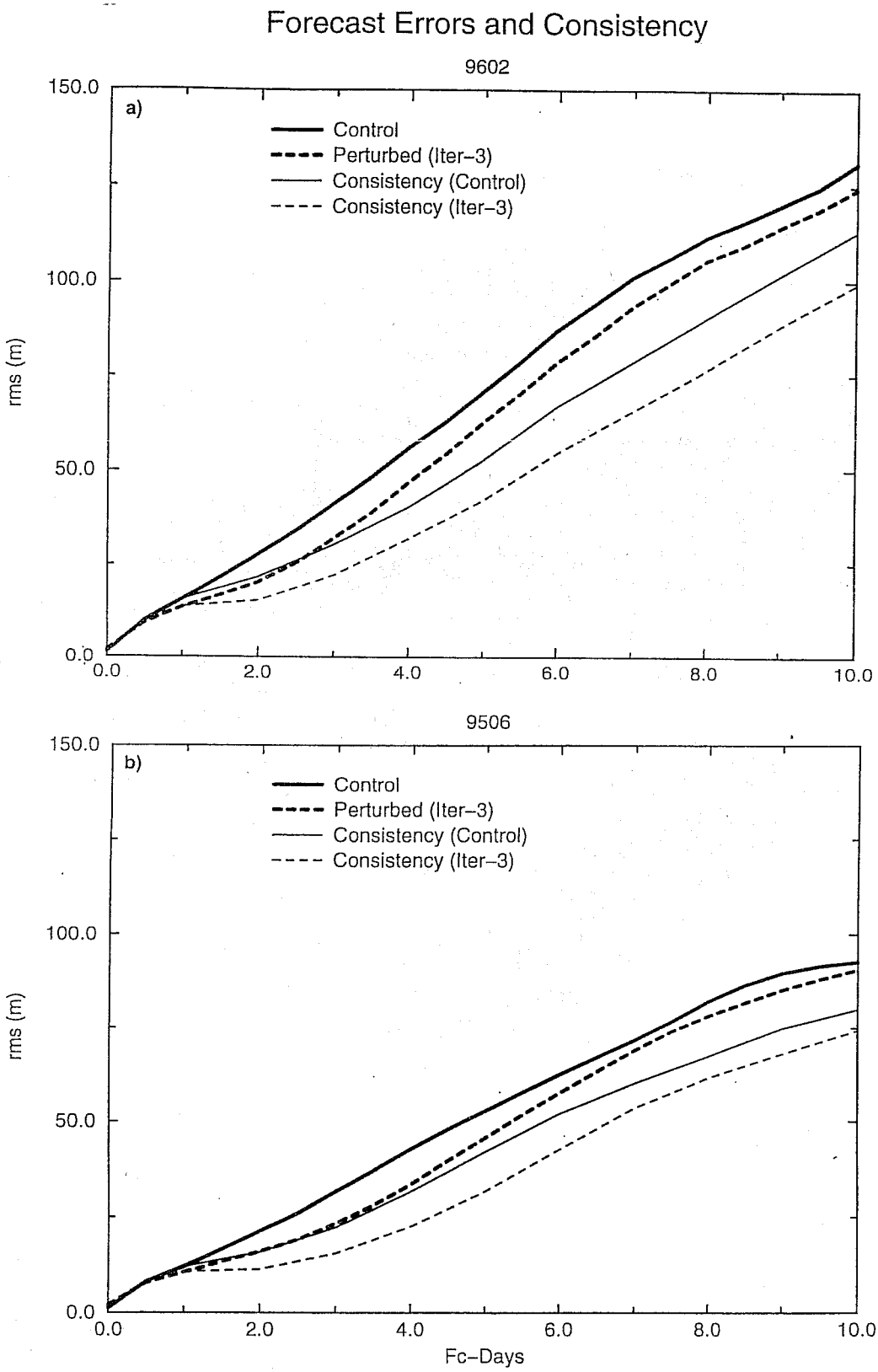


Figure 15. R.m.s. errors of control integrations (solid line) and integrations from initial conditions modified proportional to key analysis errors (dashed line). R.m.s. values of the evolution of key analysis errors (dotted line). R.m.s. differences between successive forecasts of control integrations (thin solid line) and integrations from initial conditions modified proportional to key analysis errors (thin dashed line) (a) for February 1996 (29 days) and (b) for June 1995 (20 days).

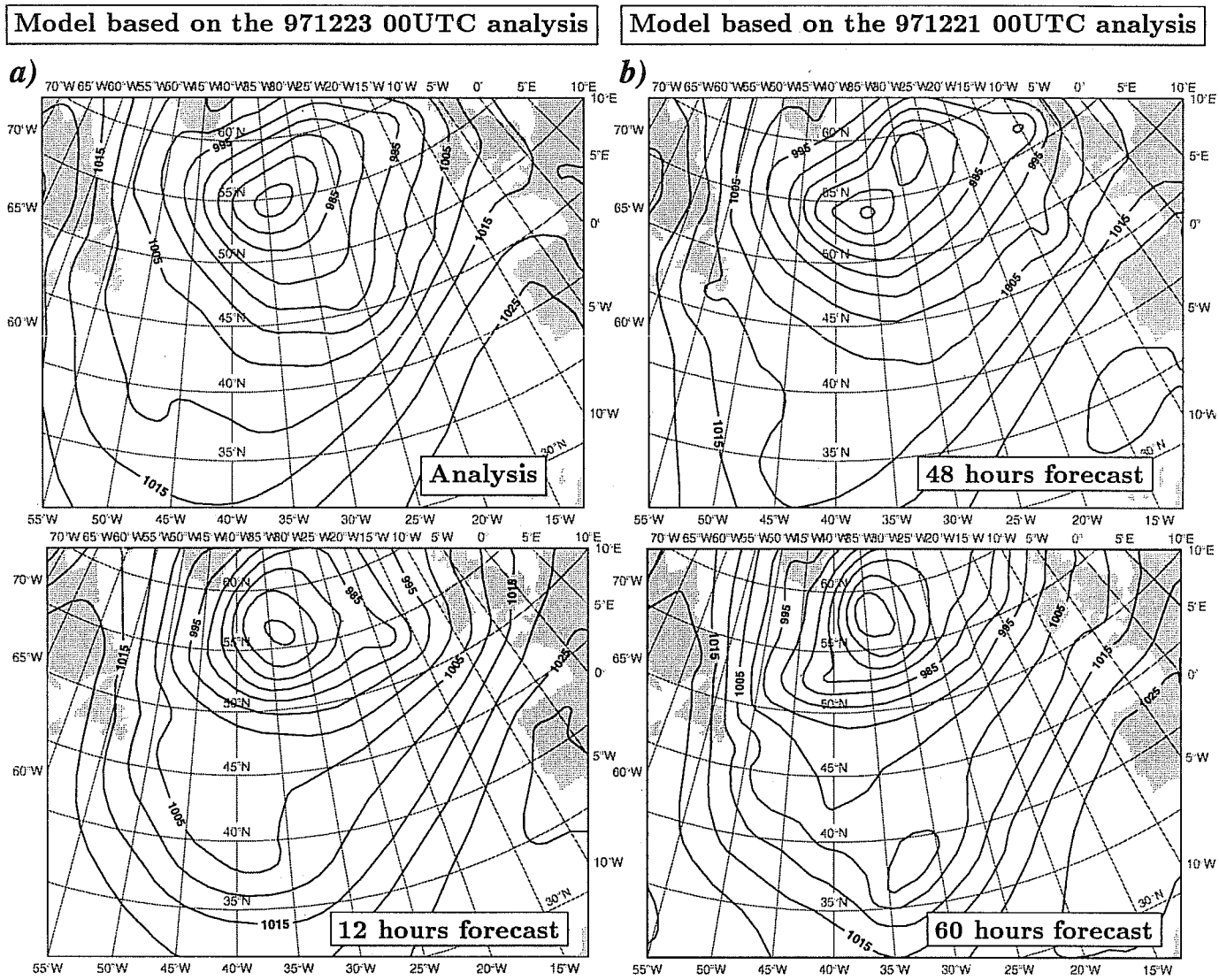


Figure 16. Comparison of the model based on the 971223 00 UTC analysis and the one based on the 991221 00 UTC analysis 48 hours later. Mean sea level pressure (hPa, contour interval of 5 hPa).

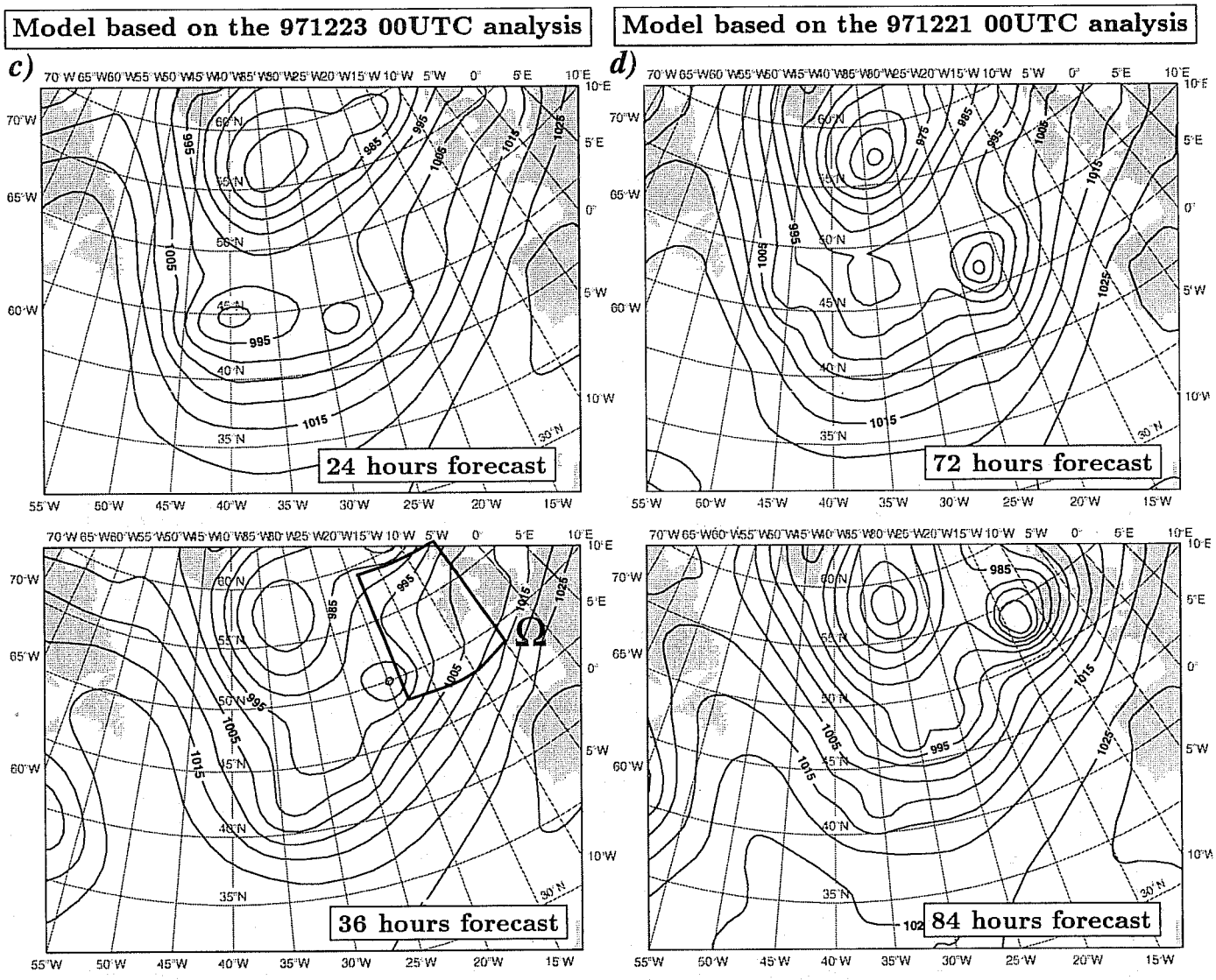


Figure 16 (cont'd). Comparison of the model based on the 971223 00 UTC analysis and the one based on the 991221 00 UTC analysis 48 hours later. Mean sea level pressure (hPa, contour interval of 5 hPa).

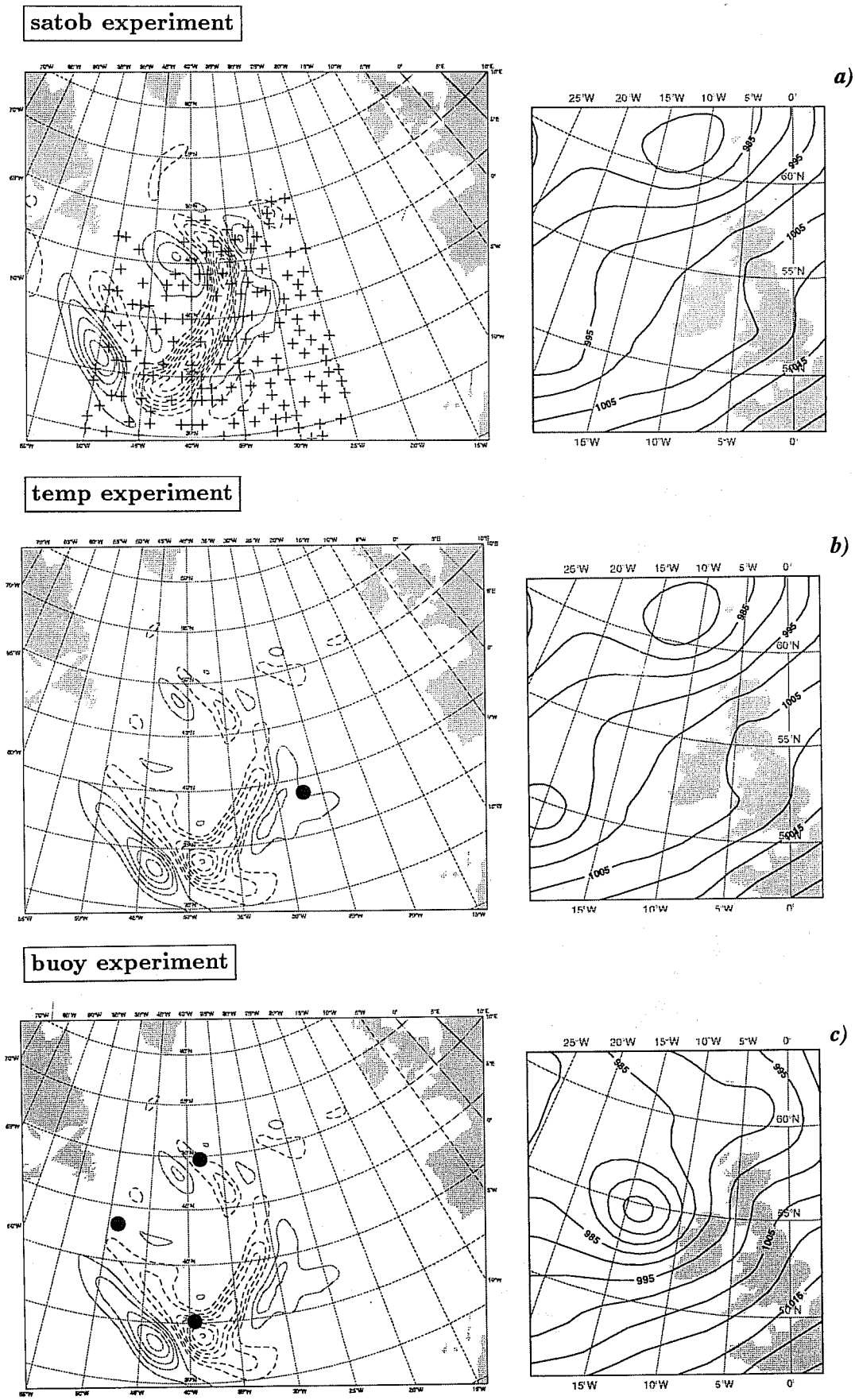


Figure 17. Experiments with perturbed analysis. Left : sensitive area and location of observations (cross or black bullet). Right : 36 hours perturbed forecast (mean sea level pressure in hPa, contour interval of 5 hPa).
a) Temperature gradient at level 700 hPa, b) c) d) Temperature gradient at level 850 hPa, e) Temperature gradient at level 500 hPa.

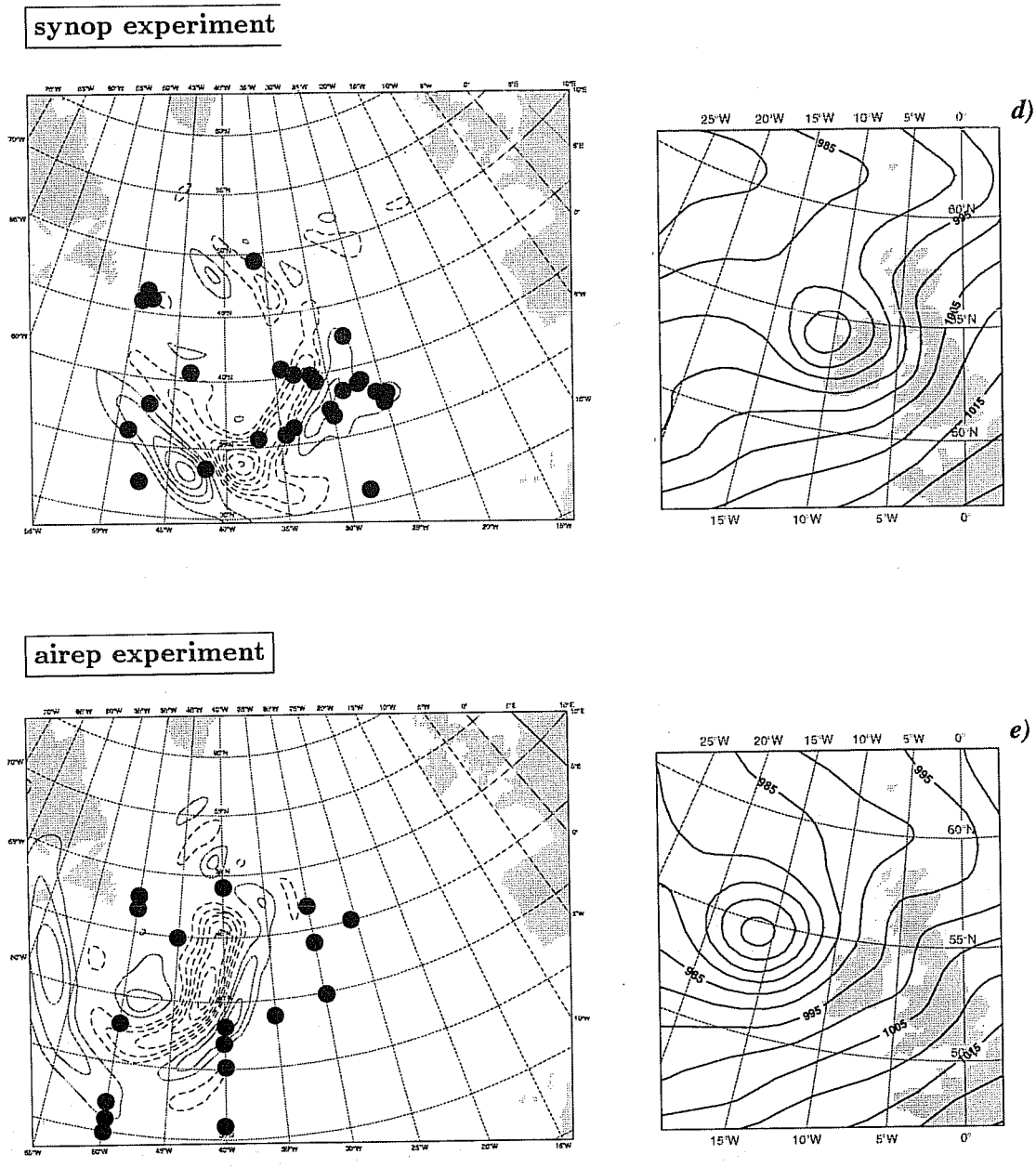


Figure 17 (cont'd). Experiments with perturbed analysis. Left : sensitive area and location of observations (cross or black bullet). Right : 36 hours perturbed forecast (mean sea level pressure in hPa, contour interval of 5 hPa).
a) Temperature gradient at level 700 hPa, b) c) d) Temperature gradient at level 850 hPa, e) Temperature gradient at level 500 hPa.